INVESTIGATION ON COMPRESSOR BLADE'S PROFILE PERFORMANCE BY USING 3D CFD

NG KONG ENG

A report submitted
in fulfillment of the requirement for the degree of
Bachelor of Mechanical Engineering (Thermal-Fluids)

Faculty of Mechanical Engineering

UNIVERSITI TEKNIKAL MALAYSIA MELAKA

2017

DECLARATION

I declare that this project report entitled "The Investigation On Compressor Blade's Profile Performance By Using 3D CFD" is the result of my own work except as cited in the references.

Signature : ....

Name : ....

Date : ....

APPROVAL

I hereby declare that I have read this project report and in my opinion this report is sufficient in terms of scope and quality for the award of the degree of Bachelor of Mechanical Engineering (Thermal-Fluids).

Signature : ....

Supervisor's Name : ....

Date : ....

DEDICATION

To my beloved father and mother.

ABSTRACT

The key of determining the aerodynamics performance of compressor rotor blade is the drag and lift coefficient. Higher lift to drag coefficient indicates that less input power required for compressor blade rotation and growth in the efficiency of compressor. However, lift to drag ratio differs regarding to the profile of an airfoil. The other factor that contributes to compressor performance is the tip leakage occurrence. Tip clearance leads to the occurrence of tip vortex at suction surface side of compressor rotor and eventually forms a blockage effect that causes compressor stalling. In this study, three dimensional twisted profiles NACA 65(2)415, NACA 65(410) and NACA 65(4)221 are utilized to investigate the most suitable profile for compressor rotor of gas turbine using the method of numerical simulation (CFD). The performances of blade profiles are also determined using graphical visualization in Fluent post-processing (CFD). Profile NACA 65(2)415 has the highest lift to drag ratio of 20.9, which is 10% higher than the other profiles. The developed wake region at the trailing edge of profile NACA 65(410) raises the drag coefficient and deteriorates aerodynamic performance. However, NACA 65(4)221 does not manifest the best result in the three-dimensional visualization of tip leakage vortex (Q-Criterion). Although vortices are formed at the tip of all profiles, the vortex formed on suction side of profile NACA 65(4)221 has the lowest turbulence kinetic energy followed by NACA 65(2)415 and NACA 65(410). This finding corroborates NACA 65(2)415 is the most suitable profile for the industrial axial-flow compressor rotor application. However, the effect of tip vortex shall not be neglected. Further investigation shall be made to control the tip vortex of NACA 65(2)415 and avoid compressor stalling and reduction in compressor efficiency.

ABSTRAK

Kunci utama dalam menentukan prestasi aerodinamik bagi rotor untuk pemampat adalah daya seretan dan daya angkat. Nisbah daya angkat kepada daya seretan yang tinggi menunjukkan kuasa yang diperlukan untuk putaran bilah pemampat adala rendah dan ia dapat meningkatkan kecekapan pemampat. Walau bagaimanapun, profil bilah yang berbeza mempunyai nisbah daya angkat kepada daya seretan yang berlainan. Faktor lain yang menyumbang kepada prestasi pemampat adalah pembentukan pusaran di hujung bilah. Hal ini menyebabkan berlakunya pusaran di permukaan sedutan pemampat pemutar dan akhirnya menyebabkan kehalangan kepada gerakan bilah pemampat. Dalam kajian ini, tiga 3D profil bilah iaitu NACA 65(2)415, NACA 65(410) dan NACA 65(4)221 digunakan untuk mengkaji profil yang paling sesuai dengan mengunakan aplikasi Pengkomupteraan Dinamik Bendalir (CFD-Fluent). Prestasi profil bilah juga ditentu melalui visualisasi grafik. NACA profil 65(2)415 mempunyai daya angkat tertinggi iaitu 20.9 ataupun 10% lebih tinggi daripada profil lain. Pemisahan bendalir di belakang bilah NACA 65 (410) meningkatkan daya seretan dan menjejaskan prestasi aerodinamik bilah pemampat. Walau bagaimanapun, NACA 65 (4) 221 tidak menunjukkan hasil yang terbaik dalam visualisasi pusaran (Q-Criterion). Walaupun pusaran dibentuk di hujung profil yang dikaji, pusaran yang terbentuk di bahagian sedutan profil NACA 65(4)221 mempunyai impak pergolakan yang paling rendah diikuti oleh NACA 65(2)415 dan NACA 65(410). Penyelidikan ini menunjukkan profil NACA 65(2)415 paling sesuai bagi pemutar bagi pemampat aliran-pakai tetapi kesan pusaran tidak harus diabaikan. Penyelidikan lanjut harus dilakasanakan untuk mengawal pusaran yang berlaku di hujung bilah NACA 65(2)415 untuk mengelakkan pengurangan kecekapan pemampat.

ACKNOWLEDGEMENT

I would like to express my appreciation to my final year project supervisor, Dr. Yusmady Bin Mohamed Arifin for his guidance throughout this research and report writing. Secondly, I am gratitude to my second examiner as well as panel, Dr. Cheng See Yuan and Dr. Suhaimi Bin Misha who gave me advices and reviews that helped me in completing this research. Lastly, I am grateful to my parents and friends who assisted me in finalizing this project within the limited time frame.

CONTENT

LIST OF FIGURES

LIST OF TABLES

LIST OF SYMBOLS

F_L	=	Lift Force, N
F_D	=	Drag Force, N
ρ	=	Density, kg/m^3
v	=	Velocity, m/s
A	=	Frontal Area, m^2
Cl	=	Lift Coefficient
Cd	=	Drag Coefficient
θ	=	Twisting angle of Blade, °

LIST OF ABBEREVATIONS

CFD	Computational Fluid Dynamics
NACA	National Advisory Committee for Aeronautics

CHAPTER 1

INTRODUCTION

1.1 BACKGROUND

The history of the first invented gas turbine has never been sorted out. However, the first registered trademark of gas turbine was by a British named John Barber. from United Kingdom in 1791. Charles Parsons, set off the idea of first patented axial flow compressor in 1884 and followed by the multistage axial compressor and turbine in 1904 (Hunt, 2011). The first successful gas turbine was developed in 1930s and the first gas turbine used for electric generation was introduced in Oklahoma in 1949 (Cengel and Boles, 2014). The gas turbine has experienced historically improvement and changes over the centuries. Today the development of gas turbine is focus within the areas of increment the temperature of turbine inlet, modification to the basic thermodynamic cycle and improvement in the efficiencies of turbomachinery components.

A gas turbine is the heart of a power plant. It can be divided to three portions which are compressor, combustion chamber and turbine. An axial compressor is selected for the usage of gas turbine is due to continuous supply of high mass flow capacity and its high efficiencies air flow. Air flows into the compressor is directed by inlet guide vanes into the stages of rotor and stator blades (Boyce, 2012). Rotors rotating in high speed produce air flow with high velocity. The flowing air is then diffused by the stator which is stationary and thereby produces high pressure. The process is repeated stage by stage and raises the overall pressure ratio of the system. Rotor and stator blades are designed based on the shape of airfoil which is an aerodynamic shape that allows any blades to be lifted. The shape of airfoil divides air flow to top and bottom of a blade. The top part of a blade usually designed in a convex curve. Compared to concave curve at bottom of the blade, the fluid flow will more streamline and this indicates that the velocity flowing on top on the blade is higher. According to Bernoulli's Principle, the higher the velocity, the lower pressure on the part of the blade. Thus, an upward force is created which allows the blade to be lifted as shown in Figure 1.

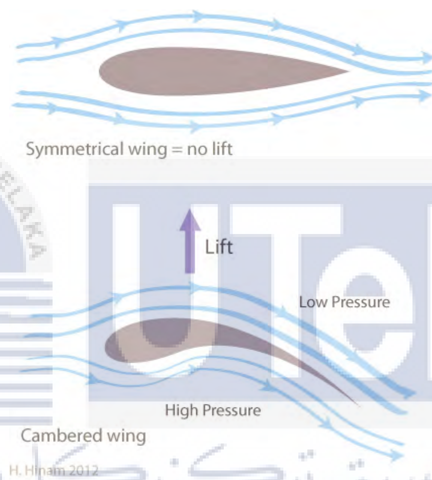

Figure 1.1 The principle behind an airfoil blade

Turbomachinery of compressor blades play an important role in the efficiencies of gas turbine. Inventors in the 1800s faced the difficulties to achieve a great performance gas turbine due to limitation knowledge in aerodynamics and financial costs. Today, with the help of advanced computational technology, simulation of turbomachinery components such as compressor blade profile and cascade are crucial in the analysis of the performance of gas turbine.

1.2 PROBLEM STATEMENT

An axial flow compressor is important in supplying high static pressure to a gas turbine. Scientists have made efforts over the centuries in raising the overall pressure ratio of the system and firing temperature in order to increase thermal efficiency of the cycle. However, the blade profile of compressor blade also plays an important role in the criteria of smoothness of the air flowing through. Thus, the analysis of a single compressor blade is remarkable to keep the air flowing smoothly and minimize the pressure loss due to friction throughout the process. The airfoil designed blade profile holds the crucial keys to determine the drag and lift coefficient of a single blade. NACA 65 was selected in this research to study their fluid flow behavior using CFD (Herrig et al., 1957). Compressor stalling is a known issue that deteriorates the performance of a compressor. One of the factors that contributes to this instability is the vortex forming at the suction side of blade due to tip clearance. Investigation was carried out to study the effect of tip clearance vortex to a single rotor blade and how it affects the compressor performance.

1.3 OBJECTIVES

1. To investigate various profiles of single twisted compressor blade in term of parameters that affect cascade blade performance by using CFD.
2. To suggest the best blade profile by comparing the blade performance.

1.4 SCOPE OF PROJECT

The scopes of this project are

1. Focus on a single twisted blade of axial flow compressor for gas turbine engine.
2. Create 3D model by using SolidWork for twisted blade of NACA 65(410), NACA 65(2)415 and NACA 65(4)221.
3. Simulate of fluid flow for a three-dimensional twisted blade to obtain velocity and pressure distribution, coefficient of lift and drag, to observe tip leakage vortex occurs around the blade by using ANSYS.
4. Compare and suggest the blade profile with the best performance.

1.5 GENERAL METHODOLOGY

1. Identify blade profile for CFD simulation. NACA 65 is used for this research because a large number of cascade performance tests were conducted using 2D wind tunnel tests to investigate the pressure contour of blade with different angle of attack and solidities (Roland and Galison, 2000). Therefore, this database is helpful in this research and NACA 65 series blades are widely used in gas turbine industries.

2. Identify suitable parameters for angle of twisted blade and angle of attack. The range of optimum angle of attack is around 10º to 20º because lift coefficient rises to maximum whereas the drag coefficient is at minimum (Patil and Thakare, 2015).

3. Develop 3D model of twisted blade using SolidWork. The standard a single NACA 65 blade profile's coordinates is obtained and imported into SolidWork. The dimension of

blade is adjusted and extruded into a 3D aerofoil. The angle of 3D blade is then twisted using flex function available in the software.

4. Identify the suitable boundary conditions for compressor blade investigation such as inlet velocity, air properties and temperature of fluid flow.

5. Simulate fluid flow around the twisted blade. The velocity distribution, pressure distribution, lifts and drag coefficient are obtained from the result of simulation using CFD.

6. The visualization of tip leakage vortices due to tip clearance occurs around the blade tip profiles are observed using CFD.

7. Choose and suggest the best profile of among the 3D twisted blades.

CHAPTER 2

LITERATURE REVIEW

2.1 Gas Turbine

Gas turbine is employed in various power plants for electricity generation. Ambient air is drawn into compressor where the air flows through multistage of rotating and stationary blade. The air is compressed at each stage and sent to combustion chamber. The pressure and temperature of air are further increased as fuel is inject and burned with the air mixture in the combustion chamber. The hot combustion product is then directed into turbine where the volume of hot gas mixture expands to cause rotation of the shaft. The power of rotating shaft is used to drive compressor to draw in more air and electric generator to produce electricity. Gas turbine obeys the law of thermodynamics and operates with Brayton cycle. Figure 2.1 shows the actual Brayton cycle of gas turbine, stage 1-2 is the compression of fresh air drawn in by compressor. The compressed gas is heated to state 3, which has the highest temperature under constant pressure condition in the combustion chamber. In state 3-7, the hot gas mixture is expanded where the work is harvested for electricity generation. The work output in state 3-5 is relatively equal to work input of 1-2 because turbine and compressor are sharing the same shaft, part of the shaft power is used to drive compressor to draw in fresh air.

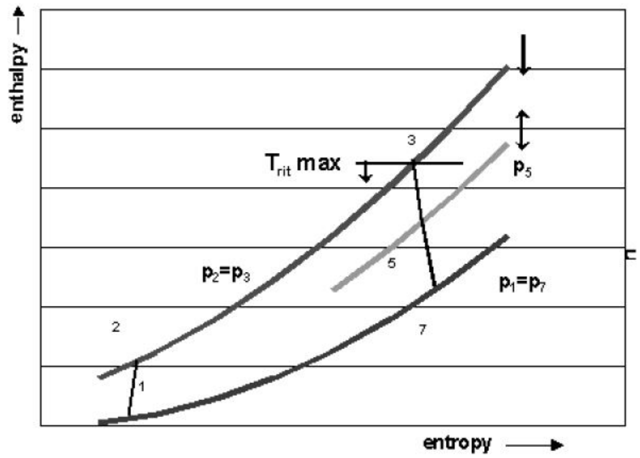

Figure 2.1 Brayton cycle of gas turbine (Brun and Kurz, 2001)

2.1.1 Compressor

Compressor is a mechanical device used to increase the pressure of flowing fluid in a certain system driven by an electric motor or combustion engine. Compressor can be divided to two categories, positive displacement and dynamic compressors. Positive displacement compressor provides continuous flow against any pressure built-up and usually employs screw, diaphragm and piston to reduce the volume of the air in the system. Dynamic compressor increases the pressure of system by converting high velocity of the air (Yusof et al., 2014). Gas turbine is in the category of dynamic compressor as it draws accelerated air into the system.

2.1.2 Centrifugal compressor

Centrifugal compressor is used in small gas turbine because it has lower flow rates compared to axial flow compressor. The fresh air is drawn in by the high speed rotating impeller and directed to its stationary diffuser. The pressure rises due to the high velocity air is forced through the impeller and diffuser. As shown in Figure 2.2, the highest efficiency of centrifugal compressor operates between the range of $90 \leq N_g \leq 850$, where N_g is the specific speed (Balje, 1964).

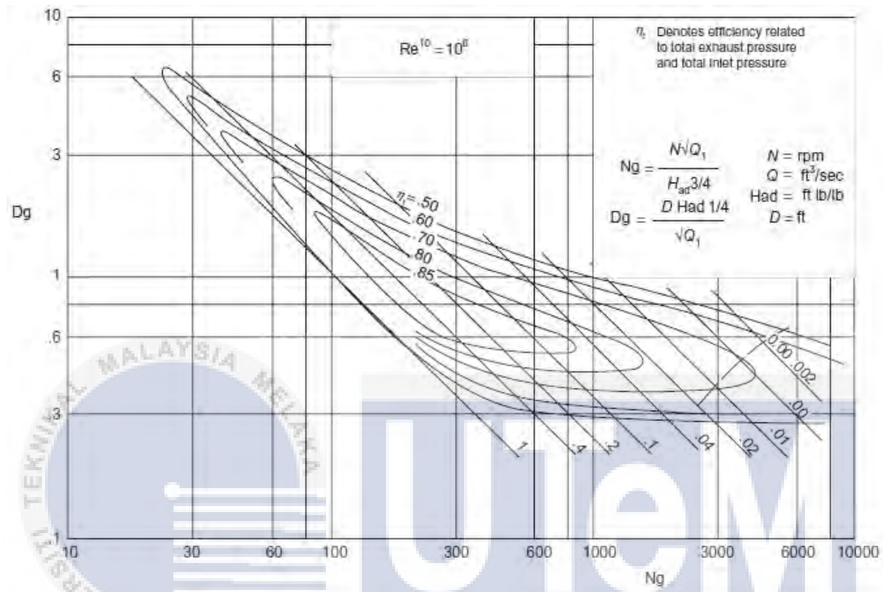

Figure 2.2 Graph of performance for typical centrifugal compressor [3]

2.1.3 Axial Flow Compressor

An axial flow compressor is another type of dynamic compressor. The air flow direction that enters and exits the compressor is parallel to the axis of its shaft rotation. The angle of air flowing into the compressor is directed by inlet guide vanes to the rotating rotor. A rotor or stator is a blade that has a shape of airfoil with the purpose of increasing its lift force. The velocity of air is accelerated and diffused by the stator of compressor. Thus, the pressure ratio of the gas turbine increases after passing of a few combination rotors and stators. This process is also known as multistage compression. The temperature, pressure and density inlet of air that draws into a transonic axial flow compressor has a range of 300–600K, 0.1-3.0MPa and 1.16-17.2 kg/m^3 respectively as shown in Table 2.1 (Ishizuka et al., 2010). Besides, the axial velocity used is 50m/s with an inlet angle 10 degree, the chord length of rotor is for a compressor blade is 0.0679m. These parameters are important for the setting of boundary conditions during numerical simulation.

Table 2.1 Parameters of inlet and outlet temperature, pressure and density of air drawing into industrial axial flow compressor (Ishizuka et al., 2010)

Compressor			Air
Temperature	(inlet – outlet)	K	300 – 600
Pressure	(inlet – outlet)	MPa	0.1 – 3.0
Density	(inlet – outlet)	kg/m^3	1.16 – 17.2

2.1.4 Compressor Blade

Compressor blade is made out of forming or machining process. The material used for fabrication is alloyed metal because the shape of compressor blade might require twisting and bending in order to reduce the load of driving force. Alloyed metal is a good option as they can be easily shaped by machining to the desired twisting angle or dimension. Compressor blades are fabricated to be durable and light weighted to draw in air while rotating at high revolution per minute. Compressor blades with rotation motion that are arranged in row inside an axial flow compressor are named as rotor while the stationary compressor blades arranged in row is named as stator. As the air flows through the rotor, its acceleration increases until it is directed to the stator. The air is losing its speed but with exchange of increasing pressure as shown in Figure 2.3.

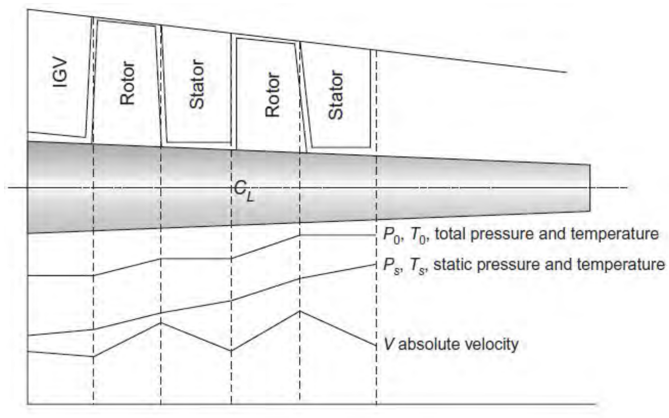

Figure 2.3 Variation of velocity and pressure plots as fluid flow through an axial compressor (Boyce, 2012)

2.2 Fluid Properties Laminar and Turbulent Flow

Laminar is well known as having a low velocity, fluid flows in highly organized compared to turbulent flow, which fluid particles flow chaotically in high velocity. There is a region where laminar or turbulent is hardly differentiate, this region is named as transition flow.

2.2.1 Separation

Separation is a phenomenon where the streamline which originally flow across a surface starting to leave the surface. According past research (Marusic et al., 2007), with the rising of angle of attack of an airfoil body, the pressure gradient will also develop and thus resulting in the formation of separation point of the airfoil. In special case, the fluid that experiences transition region where the flow rejoins to the airfoil surface after separation to form a laminar separation bubble showing in Figure 2.4 (Lian and Shyy, 2006). This transition region is difficult to simulate for all turbulence model due to indistinguishable between laminar and turbulent flow and shall be avoided. Only experiment could verify the accuracy of transition simulation (Andersson et al., 2012).

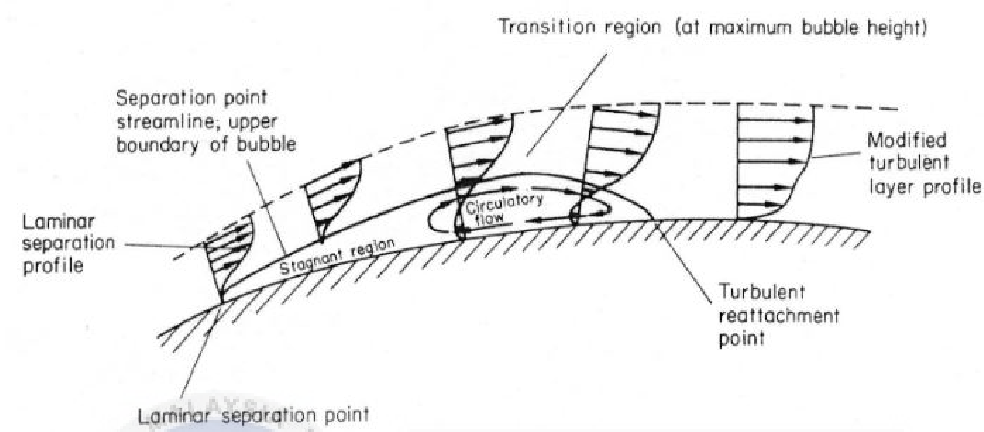

Figure 2.4 Laminar Separation Bubble formed after separation (Crivellini et al., 2013)

2.2.2 Boundary Layer over Airfoil

As illustrated in Figure 2.4, boundary layer has a velocity profile at different location of airfoil surface when it flows across an airfoil. Velocity that is in contact with airfoil surface will experience viscous effect that reduces it to zero (Sanchez, 2014). Maximize lift and minimize drag are the well-known criteria to improve the performance of an airfoil. In this case of airfoil, the boundary layer shall always adhere to the airfoil surface to prevent separation point that draws the possibility of wake region. This separation and wake region will usually occurs at the top of airfoil as the shape of airfoil favors the flow acceleration on top of blade. Eventually, the wake region will occur around the trailing edge of airfoil which yields drag over lift coefficient as the increasing pressure acted to drag direction of airfoil as shown in Figure 2.5.

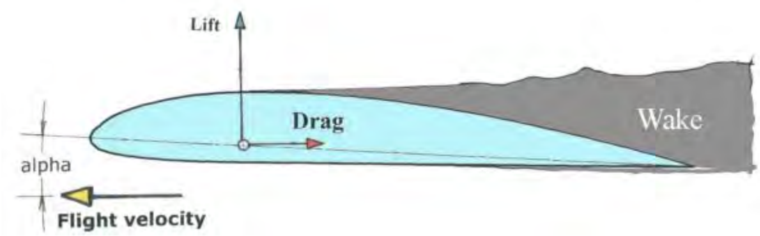

Figure 2.5 Wake region developed at trailing edge of airfoil

2.3 Blade Nomenclature and Blade Performance

A blade profile is the shape of a wing which holds the aerodynamic or hydrodynamic properties of the wing. The blade profile usually designed in the shape of airfoil to maximize the lift force and reduce the drag force of the wing. The top of the blade fabricated as a convex curve while the bottom of blade as a concave curve or flat surface. This design is to ensure that the air flowing on top it will be faster and smoother compared to the bottom of blade. With the application of Bernoulli's principle, the pressure at the bottom is dominating and results in a lift force acted on the blade. Figure 2.6 shows the nomenclature of a standard blade profile.

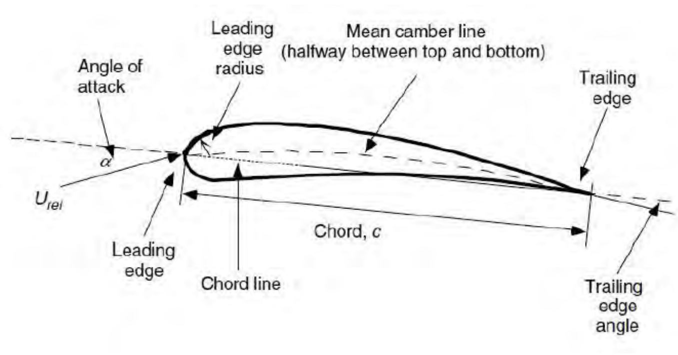

Figure 2.6 Nomenclature of airfoil blade (Boyce, 2012)

2.3.1 NACA Blade Profile

A blade profile that has shape of airfoil developed by National Advisory Committee for Aeronautics (NACA) is also known as NACA blade profile. In the earliest study, the naming of 4-series of NACA blade is followed by four digit numbers. The first digit indicates the camber, the second digit indicates the location of the maximum camber from leading edge of the blade and the last two digits represent the maximum camber thickness (Patel et al., 2015). Based on past research (Herrig et al., 1957), blade profile used for compressor blade is NACA 65. NACA 65 can be categorized to lower cambered section and higher camber section. The lower cambered section consists of NACA 65-010, NACA 65-410, NACA 65-810 and NACA 65-(12)10. NACA 65-(15)10, NACA 65-(18)10, NACA 65-(21)10, NACA 65-(24)10, and NACA 65-(27)10 are series which belongs to higher cambered section.

2.3.2 Angle of Attack

Angle of attack is the angle between the chord length of an airfoil blade and the relative motion of fluid flowing across the blade. Increasing of angle of attack of a blade will cause the rising of lift and drag coefficient at the same time. A separation region or stall region will occur when the angle of attack for a particular blade has reach sufficient large. This is usually happens when the angle of attack of the blade is larger than 15º (Cengel and Cimbala, 2014). The most suitable angle of attack would trigger a better lift to drag coefficient of a blade. Based on the past research of D.C. Panigrahi and D.P. Mishra (Panigrahi and Mishra, 2014), angle of attack with the greatest lift to drag coefficient varies widely depending on the blade profile of a particular blade. In the research, angle of attack from range 0^{o} to 21^{o} with 7 types of different blade profiles is chosen for computational simulation (CFD). The highest lift to drag coefficient occurs in a range angle of attack of 12^o to 15^o depending on the type of blade showing in Table 2.2.

Table 2.2 Highest lift to drag coefficient occurs at different angle of attack with the variation of different blade profiles (Panigrahi and Mishra, 2014)

Profile ID	Angle of Attack (Degrees)	Max. C_l	Corresponding C_d	C_l/C_d ratio
E-420	15	2.553	0.551	4.633
E-544	15	2.228	0.563	3.957
E-855	12	1.934	0.408	4.740
FX-74 L5 40	12	2.667	0.549	4.858
NACA 747A315	15	1.858	0.139	13.367
NACA 64(3)418	12	1.425	0.281	5.071

2.3.3 Lift and drag coefficient

The lift and drag coefficient are crucial in determine the performance of a blade. Engineers are interested in maximizing the lift coefficient while keeping the drag coefficient of as low as possible to increase the performance of a mechanism such as gas turbine engine, blade of airplane, axial fan, wind turbine, compressor blade, car's spoiler, etc. According to past research (Jain et al.,2015), maximum lift to drag depends mainly on the blade profile and angle of attack of an air that could reduce the wake region and thus reduce the drag coefficient. The lift and drag coefficient are defined by the equations below:

$$C_l = \frac{F_L}{\frac{1}{2}\rho v^2 A}$$

$$C_d = \frac{F_D}{\frac{1}{2}\rho v^2 A}$$

Where C_L is lift coefficient, C_D is drag coefficient,$F_L$is lift force, $F_D$is drag force, ρ is density, v is the upstream velocity and A is the frontal area of the object.

2.4 Mesh Quality

A good meshing is usually fine in size but smooth, arranged in highly organized and the number of cell shall be adequate for the processing of normal computer. The mesh quality is depends on skewness, othrogonal quality and aspect ratio of the mesh grid. To ensure the mesh quality, skewness should be less than 0.9, orthogonal quality must be kept above 0.1 and the aspect ratio should be as low as possible. This is because during the numerical solution for points that located in the middle of cells, interpolation method is used estimate for the solution. If the shape of grids is long, thin and sharp, the line connecting two neighboring centers used to estimate the midpoint will be intersected far from the point and thus causing the inaccurate prediction of solution. This type of grid will also cause longer time for convergence as the error will make the neighboring solution to regulate (Durbin and Medic, 2007). Therefore, grids which are long, thin and have high acute angle shall be avoided to improve the simulation results of CFD.

2.4.1 Boundary Conditions

Boundary condition is very important in computational fluid dynamics as it determines the inlet, outlet and wall conditions that define the computational domain. Inlet boundary condition decides where the fluid will be moving from and to, which against the direction of stationary or moving object. Inlet boundary conditions include velocity inlet, pressure inlet, mass flow inlet, etc. Outlet boundary condition determines the exit of the flowing fluid from a computational domain and it includes pressure outlet, outflow, outlet vent and exhaust fan

(Anonymous, 2006). Some boundary conditions like symmetry and axis boundary conditions can be used to reduce the calculation time of geometry provided the flow are same after splitting the geometry into halves. Wall boundary condition is one of the most important criteria for majority fluid problems. It can be divided to no-slip or slip condition. No slip condition holds the key where fluid experiences viscosity while it flows across a no slip surface whereas slip condition refers to no friction on a particular surface. In the simulation of airfoil, velocity inlet and pressure outlet are used for the air to enter and leave the computational domain as shown in Figure 2.7. No slip stationary wall is set for enclosure and the surface of airfoil to study the viscous flow across the airfoil (Newbauer and Kumpaty, 2012).

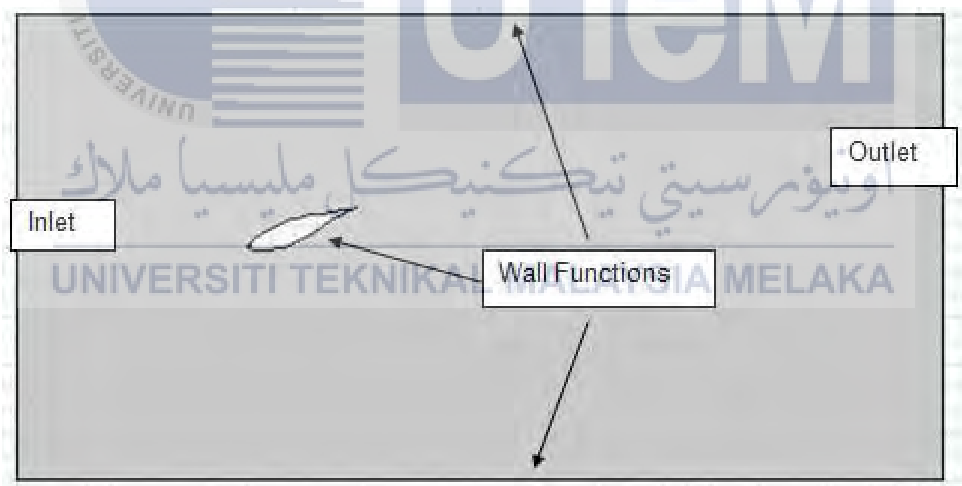

Figure 2.7 Boundary Conditions for CFD study of airfoil (Newbauer and Kumpaty, 2012)

2.4.2 Grid Independent Test

Once a simulation is converged, many will question whether if the calculation is accurate enough in term of the setting for grid size or type, discretization scheme, boundary conditions or model. Grid independent test serves the purpose of conducting a few testing in variation on the calculation set up to gain confidence in the uncertainty of simulation. For example, discretization schemes of first order and second order upwind are usually questioned for their accuracy to the solution. First order upwind is more stable and robust and it converges faster compared to second order upwind discretization scheme. However, second order upwind has a better accuracy to the approximation solution (Versteeg and Malalasekera, 2007). The idea can be concluded is the usage of first order upwind as the starting of calculation but second order upwind is used for the solution to converge in order to predict result with better accuracy. The second example is the refinement of mesh size that to test the consistency and accuracy of the solution. A coarse meshing is usually to get a rough approximation of a solution. However, to improve the accuracy of the calculation, finer meshing will be applied and the result will be used to compare with the previous coarse meshing. When the solution has come to a small change between the meshes, the grid independence is achieved.

2.4.3 Turbulence Modeling

Turbulent flows are happened in the surrounding of our daily life. Engineers are interested to study and predict the flow behavior of turbulent in order to enhance the quality of certain engines such as gas turbine, chemical reactors, heat exchanger, etc. Computational Fluid Dynamics holds the possibility to predict this type but choosing a turbulence model is crucial in interpreting the flow correctly. The procedure of choosing a correct turbulent model is shown in Figure 2.8.

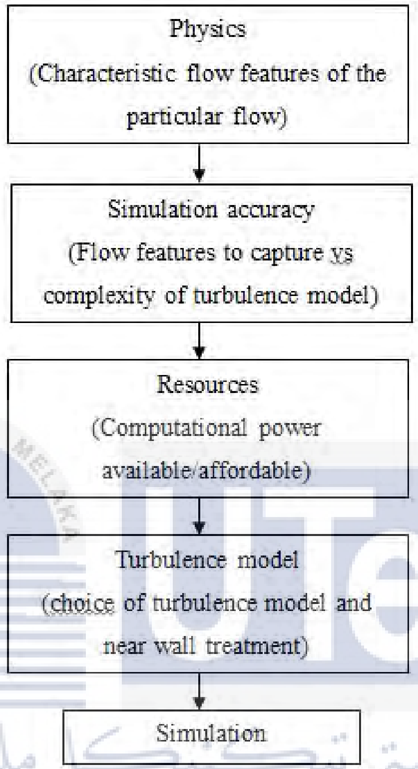

Figure 2.8 Flow chart of selection modeling process (Andersson et al., 2012)

2.5 Tip Leakage

Tip leakage occurs at the tip of rotor of a gas turbine. This phenomenon happens because of the pressure difference between suction and pressure side of blade. The flow air accelerates in to a tiny clearance, also known as tip clearance, between the wall of compressor or turbine casing and the tip of the blade as shown in Figure 2.9. The tip leakage is compressed into a narrow stream between the wall of casing and separation region, where turbulent flow is formed (Bindon, J.P., 1989). These vortices results in “blockage” around compressor rotor because the lack of effective flow path for air to circulate and ultimately causes stalling of compressor according to past research (Khalid, 1995). The tip clearance increases, tip leakage vortex forming at suction side of blade also increases due to the rising of leakage mass flow. Based on past research paper (Azad, et al., 2000), the tip clearances for gas turbine has three measurement which are 1%, 1.5% and 2.5% of the blade height. The other journal paper (Giridhar, et al., 2012) suggests that the tip clearance to blade height ratio of the axial compressor rotor ranging from 1% to 4% due to manufacturing difficulties

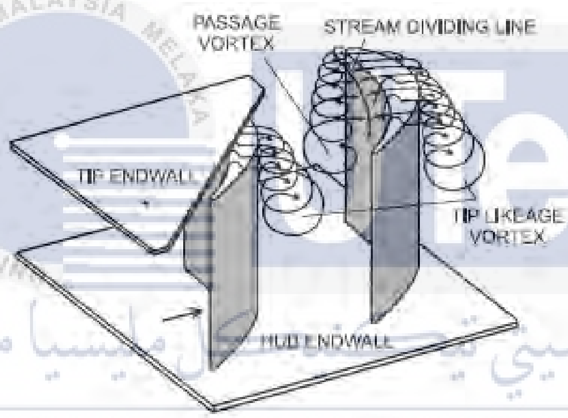

Figure 2.9 Tip leakage occurs between the blade tip and wall of casing (Lampart, P., 2006)

CHAPTER 3

METHODOLOGY

3.1 Introduction

This chapter describes the methodology used in this project to get simulation result from Computational Fluid Dynamics (CFD) regarding to the subject of study. The flow chart is displayed in Figure 3.1. To start the project, a 3D twisted blade is needed. Due to the difficulty to draw a blade profile that is highly curvature, a simple way is introduced by importing a 3D twisted blade into Ansys Design Modeler. A test section of wind tunnel encloses the blade is created as simulation domain. Each surface of the enclosure or domain is given name to define the boundary condition of the simulation. Meshes are inserted into the interior of wind tunnel. Boundary conditions and solver are defined in pre-processing of Ansys simulation. If there is problem exists in setting, the model, meshing or boundary conditions has to be rechecked. The calculation is performed and result is obtained in Ansys solution and results post-processing.

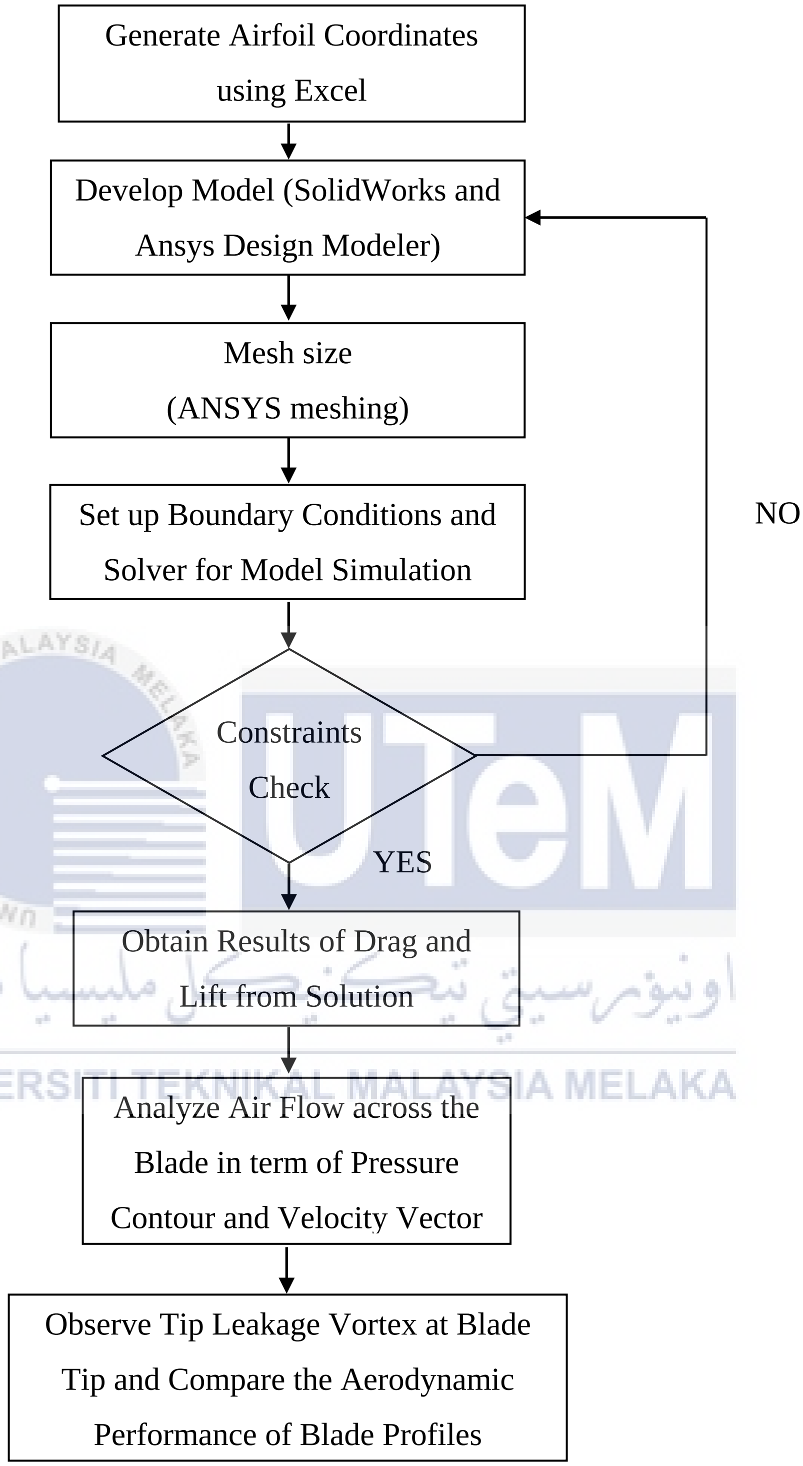

Figure 3.1 Methodology used to obtain the result from CFD simulation

3.2 Blade Profile Dimension Determination

The airfoil coordinates of NACA 65(410) that is retrieved from http://airfoiltools.com/ requires processing in Microsoft Excel to get the desired dimension or size of airfoil blade. In this case, a blade of chord length which is 100mm is needed and thus coordinates are multiply by 100 as shown in Figure 3.2. The airfoil coordinates is then saved in text file to be imported later into SolidWorks. Since an axis is required for the 2D blade profile to twist in SolidWorks, a line coordinates is created, also saved in form of text file as shown in Figure 3.3. Note that the length of this line also represents the length of the blade profile which is 500mm.

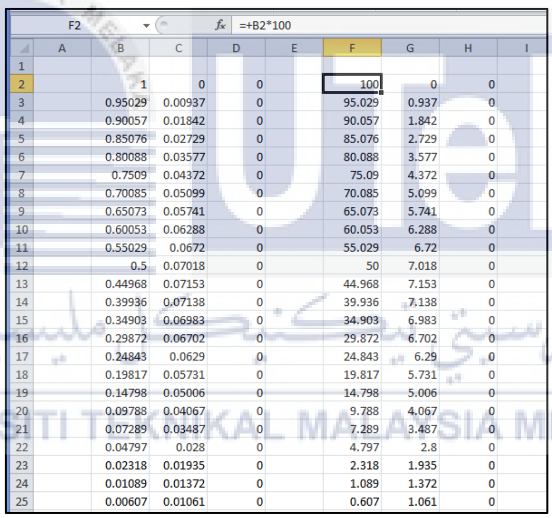
F2 =+B2*100

	A	B	C	D	E	F	G	H	I
1									
2		1	0	0		100	0	0	
3		0.95029	0.00937	0		95.029	0.937	0	
4		0.90057	0.01842	0		90.057	1.842	0	
5		0.85076	0.02729	0		85.076	2.729	0	
6		0.80088	0.03577	0		80.088	3.577	0	
7		0.7509	0.04372	0		75.09	4.372	0	
8		0.70085	0.05099	0		70.085	5.099	0	
9		0.65073	0.05741	0		65.073	5.741	0	
10		0.60053	0.06288	0		60.053	6.288	0	
11		0.55029	0.0672	0		55.029	6.72	0	
12		0.5	0.07018	0		50	7.018	0	
13		0.44968	0.07153	0		44.968	7.153	0	
14		0.39936	0.07138	0		39.936	7.138	0	
15		0.34903	0.06983	0		34.903	6.983	0	
16		0.29872	0.06702	0		29.872	6.702	0	
17		0.24843	0.0629	0		24.843	6.29	0	
18		0.19817	0.05731	0		19.817	5.731	0	
19		0.14798	0.05006	0		14.798	5.006	0	
20		0.09788	0.04067	0		9.788	4.067	0	
21		0.07289	0.03487	0		7.289	3.487	0	
22		0.04797	0.028	0		4.797	2.8	0	
23		0.02318	0.01935	0		2.318	1.935	0	
24		0.01089	0.01372	0		1.089	1.372	0	
25		0.00607	0.01061	0		0.607	1.061	0	

Figure 3.2 Enlarging coordinates of airfoil in Microsoft Excel

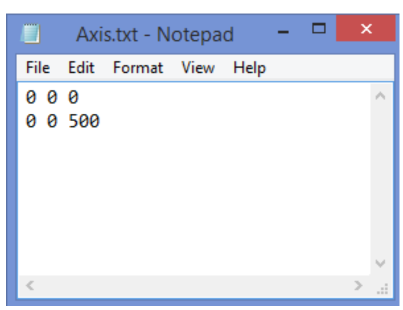

Figure 3.3 Axis of blade is created using Notepad

3.3 Creating the twisted 3D blade profile in SolidWorks

To create a twisted 3D blade profile, 2 text files that are saved earlier will be imported using Curve feature highlighted in red circle of SolidWorks in Step 1 of Figure 3.4. Swept Boss/Base in SolidWorks has a feature to extrude and twist a 2D airfoil when a profile and path are provided showing in Step 2 in Figure 3.4. In this case the 2D blade profile coordinates that is imported will be the profile, and the axis coordinates will be path as shown in Figure 3.5. 14º is set for angle of twist, θ because the best lift to drag coefficient for various profiles after pre-test of CFD simulation, fulfilling the condition within the range of 12 º to 15 º as established in Table 2.2 (Panigrahi and Mishra, 2014). Angle of twist refers to the angle between the hub profile and tip profile showing in Figure 3.6.

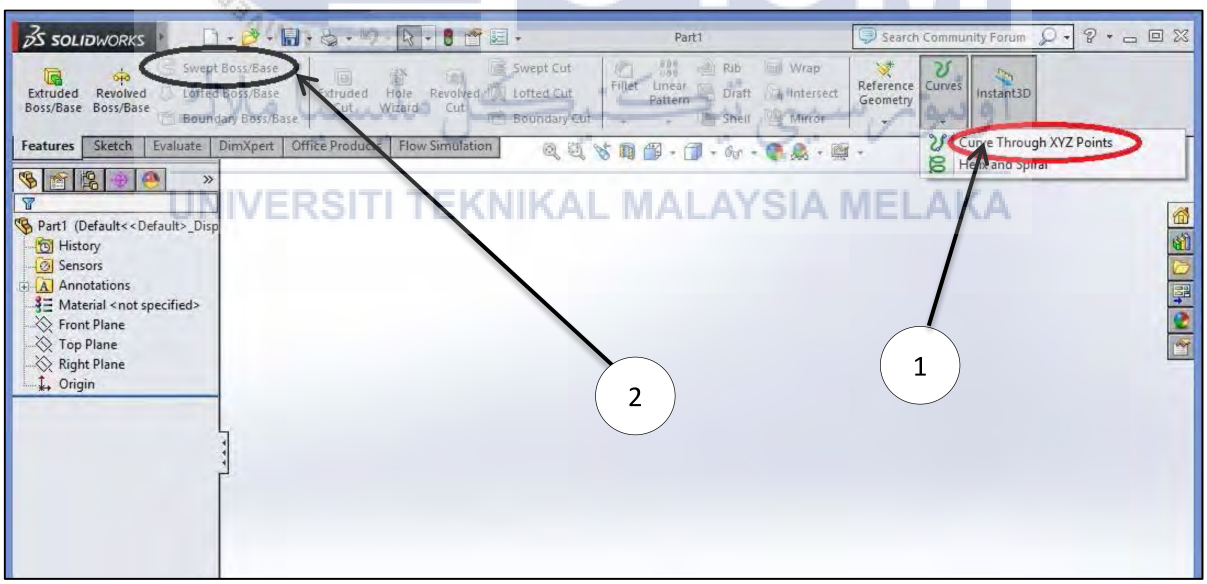

Figure 3.4 Procedures to import coordinates and create 3D twisted blade

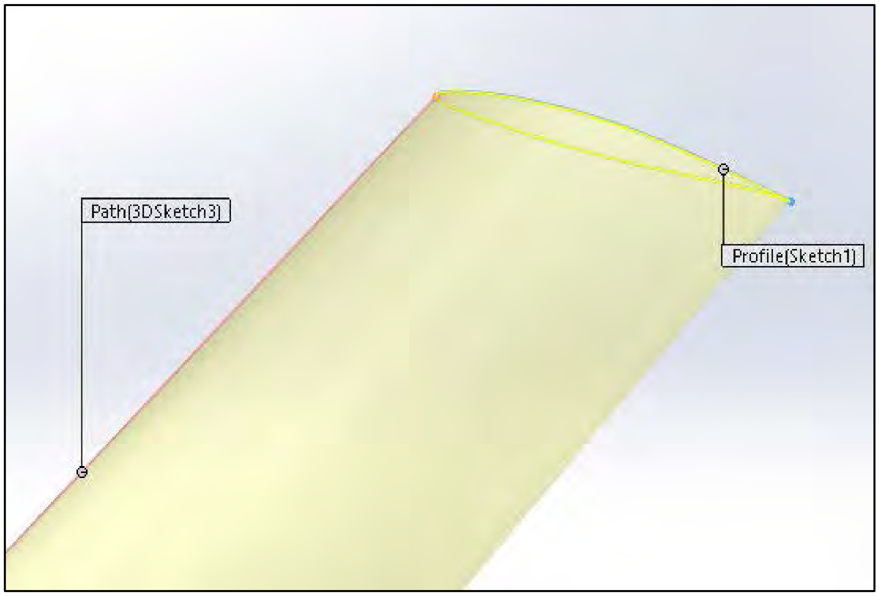

Figure 3.5 Profile of and Path selected for Swept Boss/Base and its end result

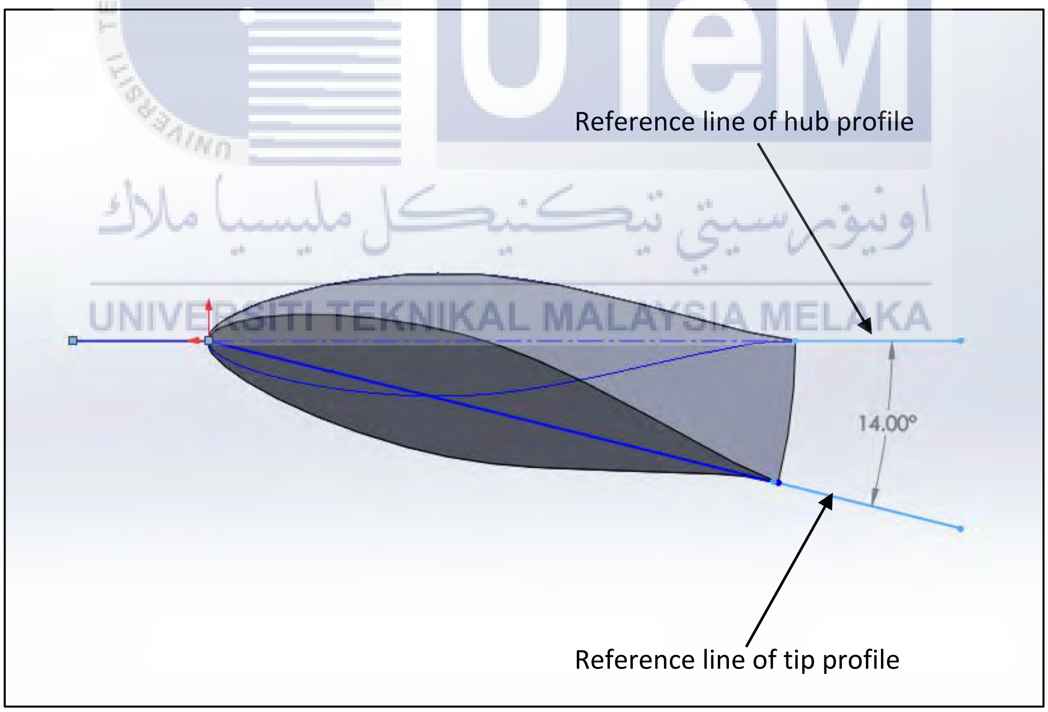

Figure 3.6 Angle of Twist, θ between Hub Profile and Tip in 2D side view

3.4 Design a test section of Wind Tunnel using Design Modeler

The blade designed in SolidWorks is imported into Ansys Design Modeler. A computational domain or wind tunnel which encloses the 3D twisted blade is created in Design Modeler with a dimension 1m × 0.505m × 0.5m by extruding a pre-drawn rectangle as shown in Figure 3.7. The width of wind tunnel is constructed as 0.505m because the blade occupied 0.5m of the width, a clearance of 5mm is taken into consideration for the analysis of tip leakage. The gap of tip clearance should be 1%, 1.5% or 2.5% of the blade span regarding to past research (Giridhar, et al., 2012). 1% (blade span) tip clearance is chosen in this study because a larger tip clearance would generate greater tip vortex. Thus, 1% tip clearance, which is also equal to 5mm tip clearance, is utilized in this study.

Blade Profile is removed from Wind Tunnel using the feature Boolean Subtract since only the air flowing across the blade is interested. Boundary conditions of compressor's walls, blade, inlet and outlet of air flow are defined using the feature Name Selections. The naming of each surfaces are shown in Figure 3.8, where A and B refer to "velocity_inlet" and "pressure_ outlet", C refers to "ns_wall", D represents "fs_wall" and E indicates "blade". Surface A is defined as velocity inlet because air enters the computational domain through this surface. B refers to pressure outlet indicates that the flow exit the computational domain through this surface. Surfaces C are non-slip wall. The inner surface is the casing wall of the compressor while the outer surface is the hub of the blade. Since the tip leakage occurs between the blade tip and casing wall, where fluid friction takes place. Thus, it is crucial to define the casing wall as non-slip wall in order to the surrounding fluid flow. The blade hub is defined as non-slip wall due to the developing of boundary layer while air enters the compressor in real situation. This setting creates the same conditions as real situation. Surface D is the free slip wall of the axial flow compressor. It does not consider as a true wall since there is no friction and viscosity on this surface. Surface E is the blade surface and is defined as non-slip wall. This is the crucial part as when fluid flows through the blade surface, the blade viscosity causes friction between air and the blade resulting in pressure gradient.

For the purpose of minimizing number of elements using in meshes, a boundary surrounded the blade is created as a selection for body of influence showing in Figure 3.9. The sketched layer is extruded as “add frozen”.

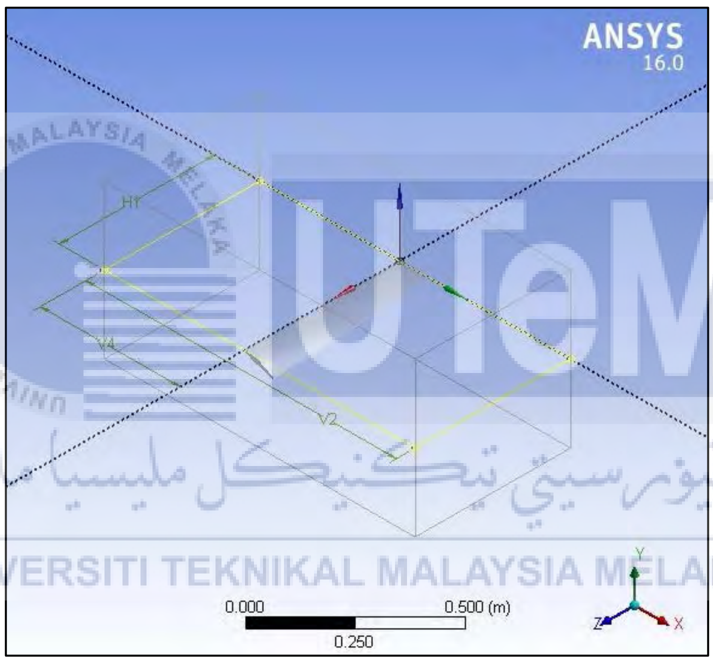

Figure 3.7 Rectangle drawn on ZX Plane is extruded to form 3D Axial Flow Compressor

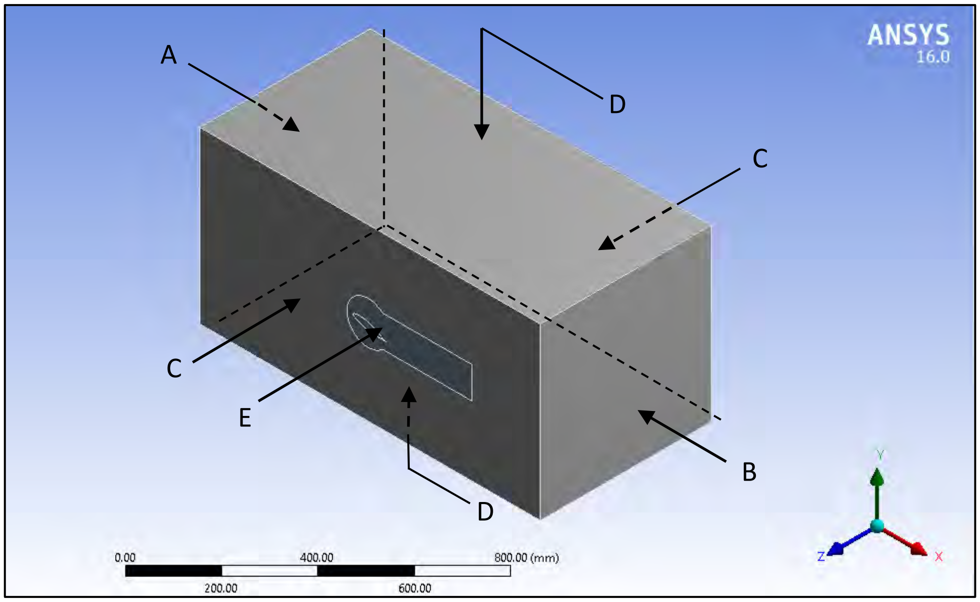

Figure 3.8 Defining each surfaces of computational domain with name selections

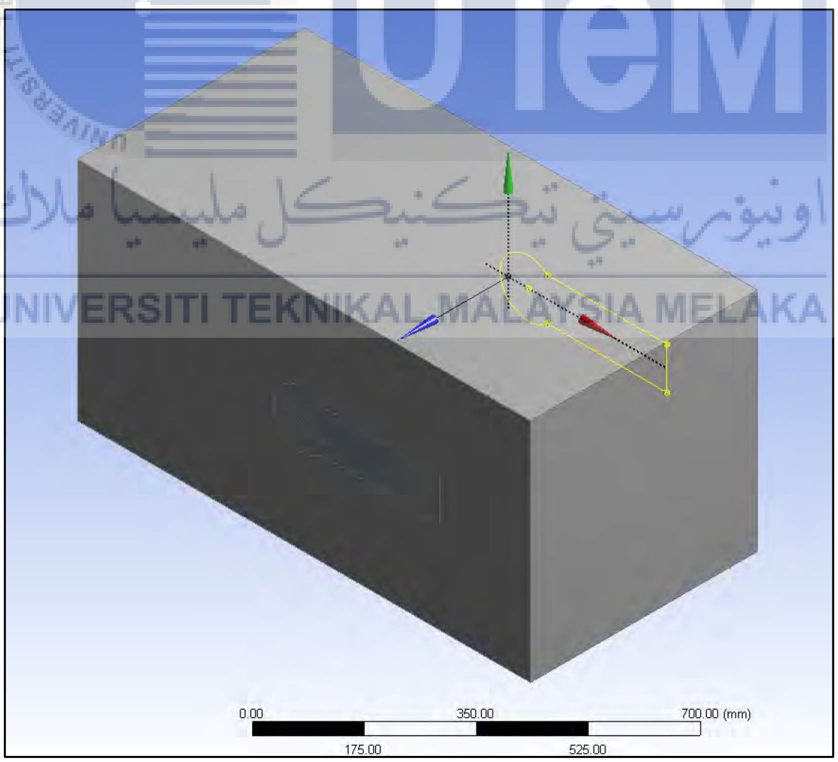

Figure 3.9 Sketch created surrounding blade for the purpose of Body of Influence

3.5 Setting Mesh for Interior of Axial Flow Compressor

Meshing is the generation of multiple nodes in a computational domain. It is critical in determining the air behavior while it flowing across the 3D twisted blade since the approximation calculation is based on the quality of mesh. The meshing used on this blade is face sizing and body of influence as shown in Figure 3.10. Body of influence minimizes computer resources as processing load is only focus in meshes surrounding the blade, which is also the area of interest where flowing fluid arises. Face sizing helps in mapping the meshes around the edges and the surfaces of blade. Face sizing also preserves the quality of meshes in term of skewness, orthogonal quality and aspect ratio. The element size used for body of influence and face sizing are 4mm and 2.5mm respectively. Whole elements of meshes are displayed in three dimensional view and side view showing in Figure 3.11(a) and (b). The computational domain is mapped with an average of 3 million elements for each blade profile. Figure 3.12 shows the meshing of 1mm tip clearance and blade surface using face sizing.

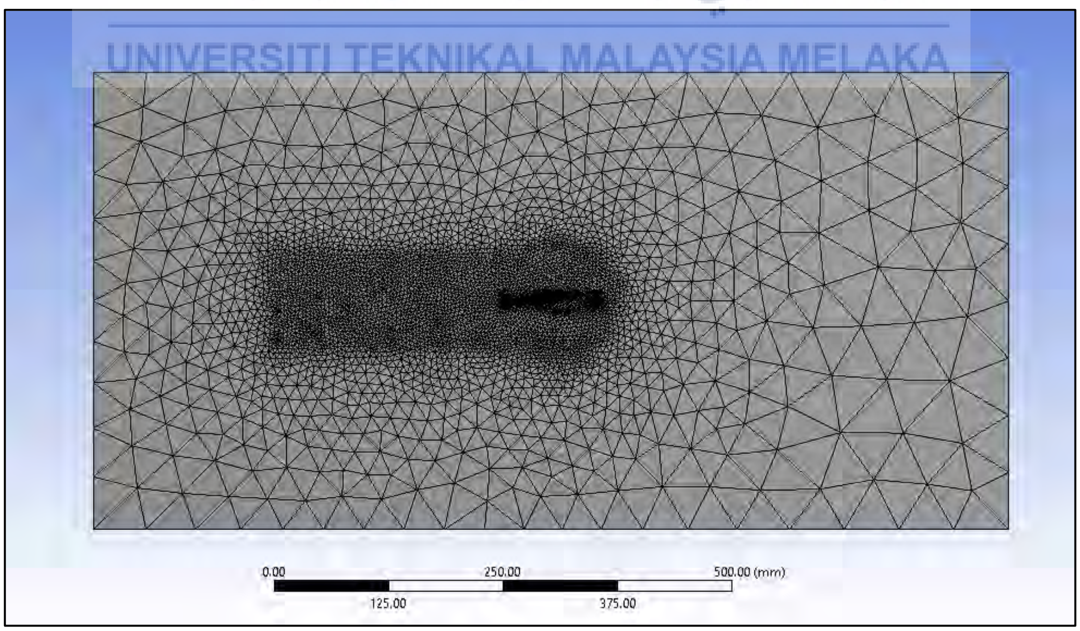

(a)

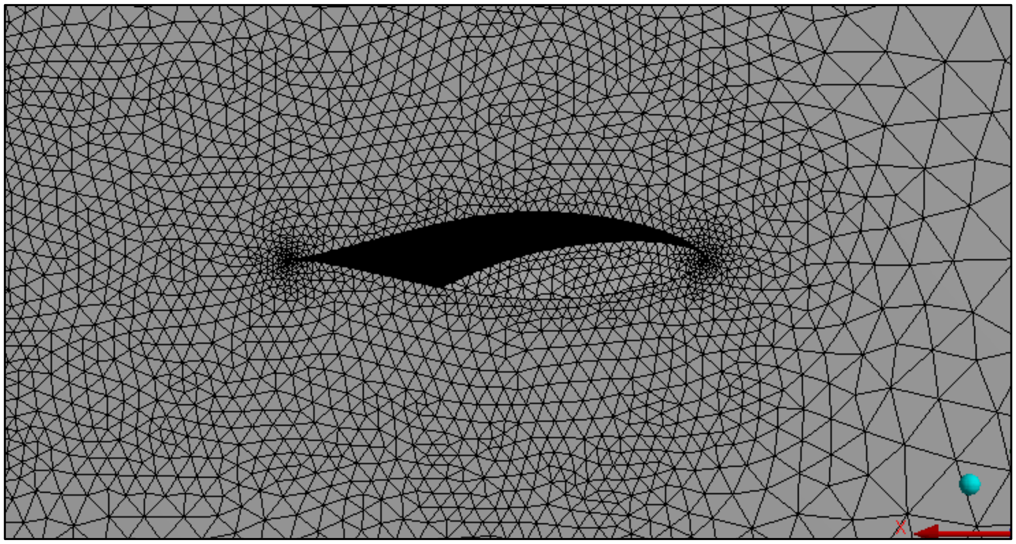

(b)

Figure 3.10 (a) Face Sizing and (b) Zoomed View of Body of Influence surrounding blade

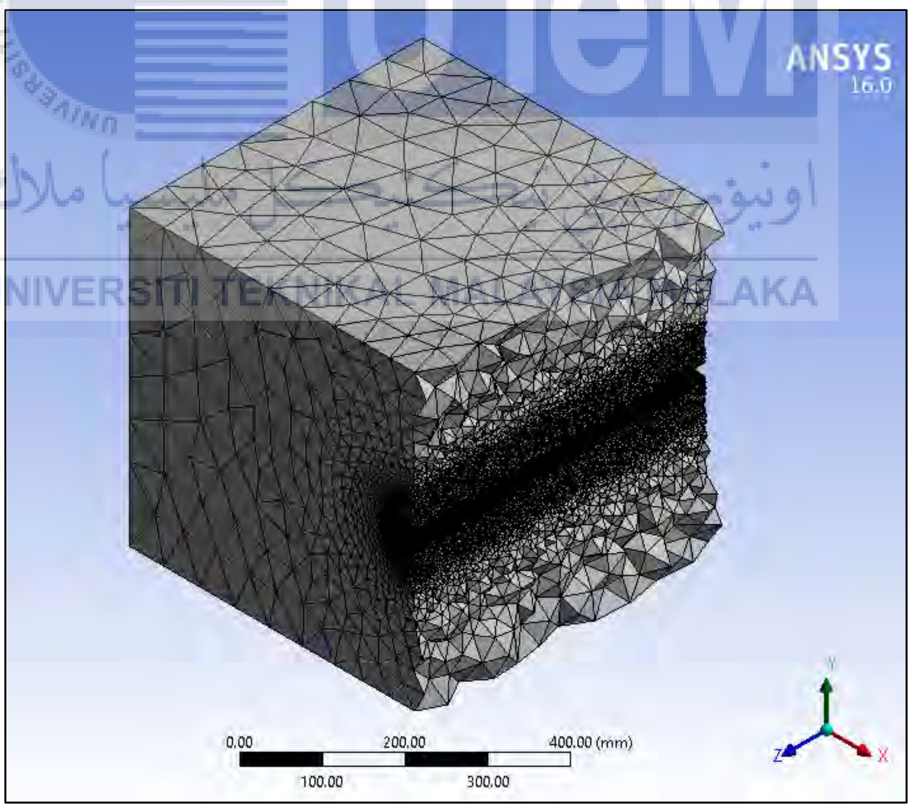

(a)

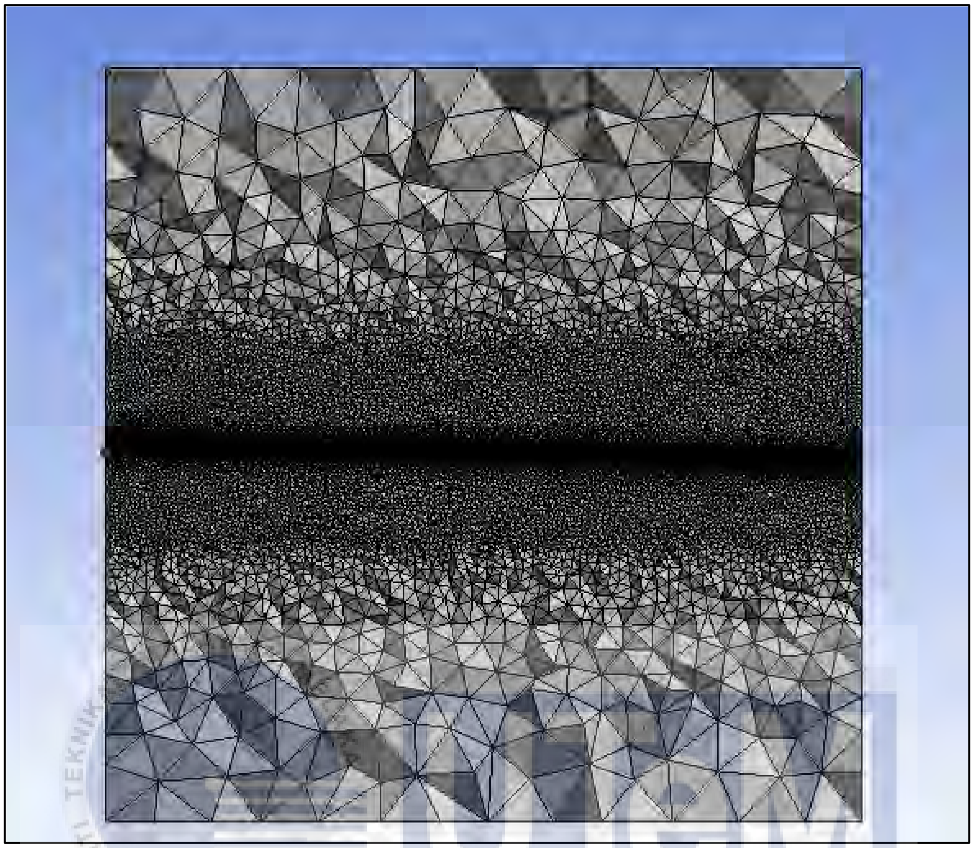

(b)

Figure 3.11(a) Isometric View and (b) Side View of Section Plane Meshing

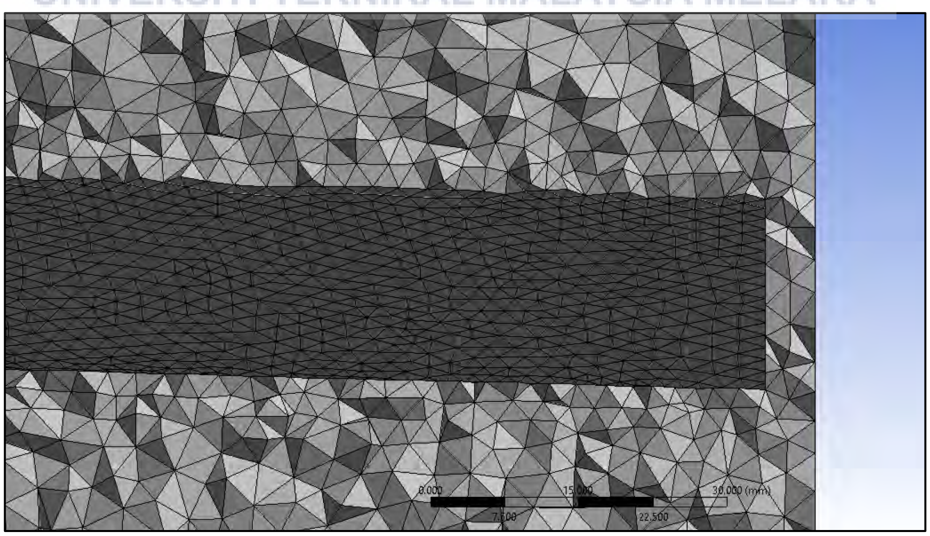

Figure 3.12 Meshing of Tip Clearance and Blade Surface

3.6 Setting Turbulence Model, Boundary Conditions, Cell Zone Conditions, Solution Methods, Monitors and Iterations used for Simulation

Before proceeding to select turbulence model, the mesh quality is checked to ensure accurate calculation result as shown in Step 1 Figure 3.13. To ensure the mesh quality, skewness should be less than 0.9, orthogonal quality must be kept above 0.1 and the aspect ratio should be as low as possible. High skewness causes distortion in shape of meshes resulting in poor approximation to the solution. High aspect ratio indicates that the cell size undergoes large changes in cell size. This results to inaccurate interpolation due to the large gap between edges of cell.

The simulation is selected as Pressure-Based, Steady and Absolute Velocity Formulation under General tab. For the turbulence model, standard k-ε is chosen to study separation and wake region across the blade because it predicts kinetic energy, k and turbulent dissipation, ε. Although k-ε is not suitable for the simulation of complex flow, but it gives reasonable solution and it does not require heavy computing resourses. Standard wall function is enabled under near wall treatment showing in Step 2. Air is selected as the flowing fluid, the density, specific heat, thermal conductivity and viscosity is set as the desired parameters in Materials, Step 3 of Figure 3.13. Air is chosen in the Cell Zone Conditions as air is the working fluid taken into compressor showing in Step 4.

In Step 5 of Figure 3.13, "blade" defined earlier is selected as non-slip stationary wall. Repeat the same procedures for "ns_wall" as the wall has shear stress. "velocity_inlet" is chosen as velocity inlet as air will enter computational domain through this surface.. Inlet velocity of 18m/s is set. Pressure outlet is chosen for "pressure_outlet" where the air will leave the computational domain. "fs_wall" has specified shear condition, the wall roughness is set to zero as shown in Figure 3.14. In Step 6, the reference values is computed from velocity inlet and frontal area of the blade is inserted in order to get accurate result of simulation. For the three profiles studied, the frontal area have similar value of $0.0125m^2$ calculated using formula of trapezium based on the front view of blade from drawing as shown in Figure 3.15.

Before running any calculation, drag and lift coefficient the key results to be studied in this simulation. in turned on in monitors under Step 7. For starting, Hybrid Initialization is ran and First Order Upwind is set for the first 100 iterations. Once the calculation is completed, rerun the calculation with Second Order Upwind until the solution is converged as in Step 8, Figure 3.13. This is because the usage of First Order Upwind stabilizes the calculation at starting but Second Order Upwind provides a more accurate result. Thus, Second Order Upwind is used to until the solution is converged.

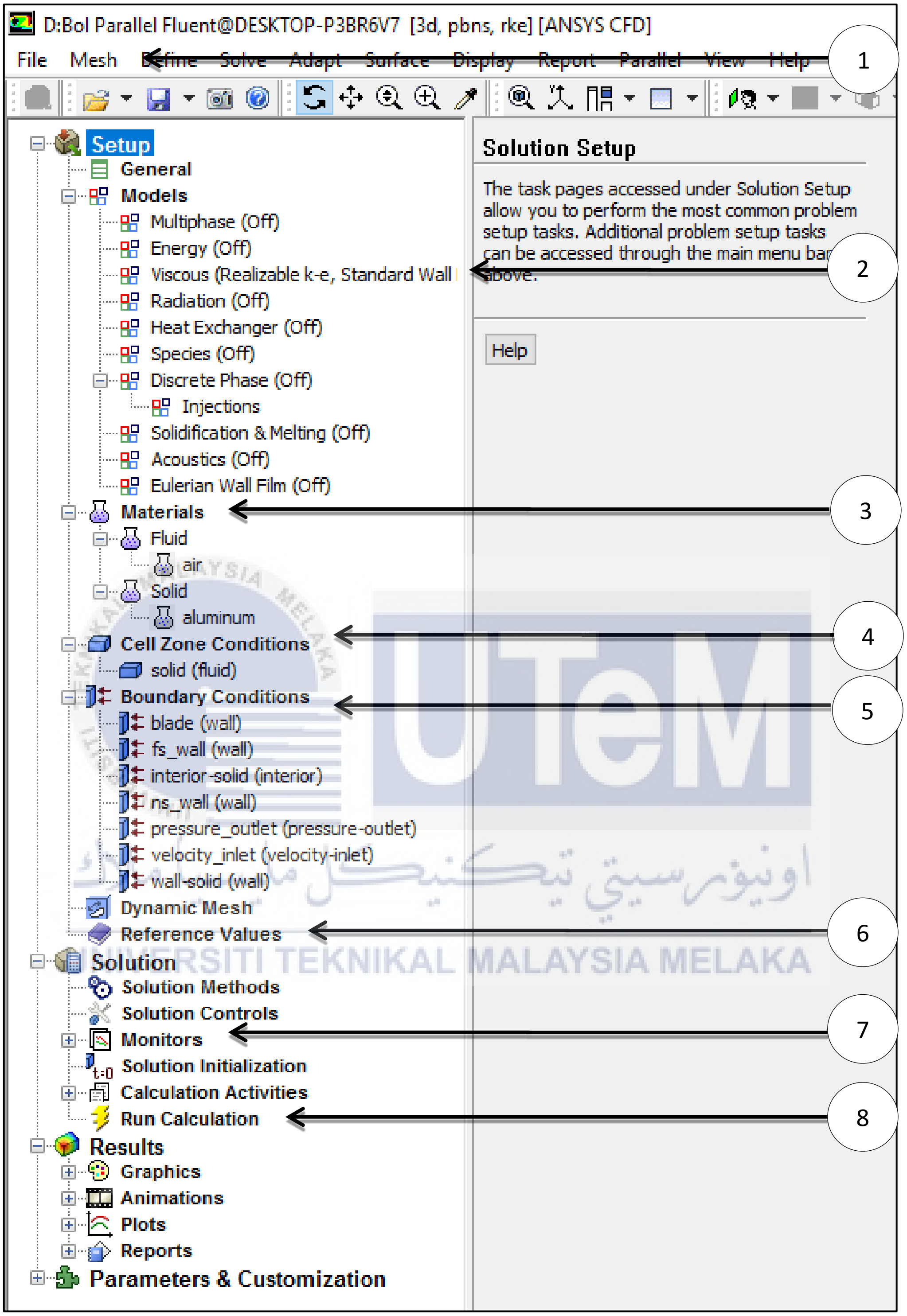

Figure 3.13 Setting for Calculation and Displaying Results

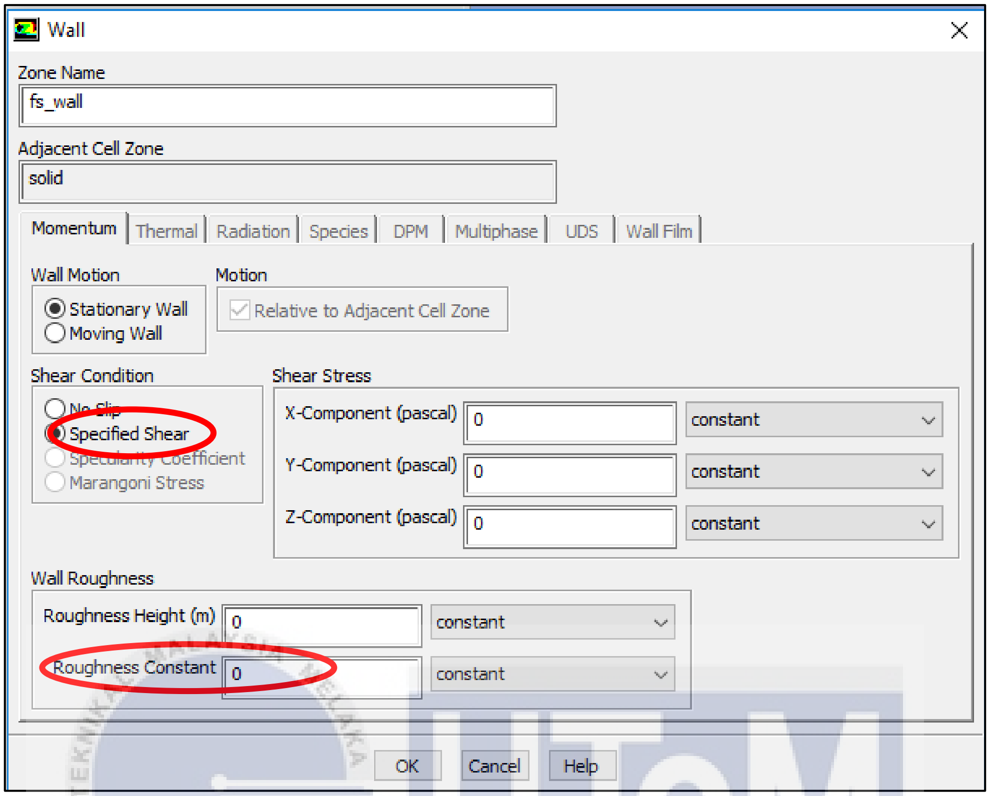

Figure 3.14 Setting for Free Slip Wall Boundary Condition

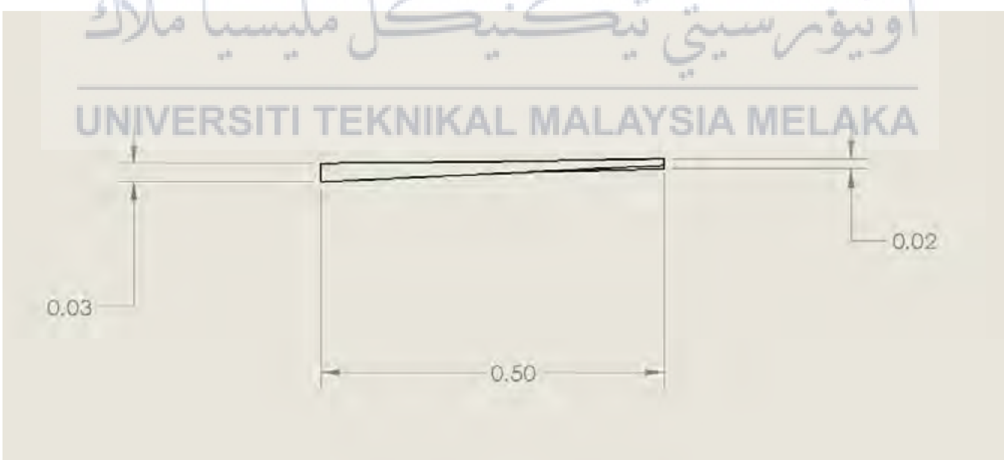

Figure 3.15 Front View of Blade from SolidWorks Drawing

3.7 Results Display and Analysis

Analysis of the results can be categorized to visualization and numerical. Visualization denotes the observation of flow behavior, velocity vector and pressure contour around the studied blade profiles. For the ease of data visualization analysis, the case and data for every profile, NACA 65(2)415, NACA 65(410) and NACA 65(4)221 are exported and loaded within a single Fluent Result. Since the area of interests is difficult to be displayed in three-dimensional view, two-dimensional view at selected blade span is inserted and displayed. By synchronizing camera in displayed views, the visualization results for all blade profiles can be analyzed easily since all the windows follow the same camera view showing Figure 3.16. The two-dimensional view of pressure contour or velocity vector of blade can be analyzed at desired segment of blade span conveniently.

Tip leakage is another factor that affects the compressor performance. Visualization of tip vortex is important in determining the compressor performance. In post processing of Fluent, vortex core region is utilized to observe the location of vortices occurred surrounding the blades for NACA 65(2)415, NACA 65(410) and NACA 65(4)221. Table 4.3 displays the visualization result as front view of axial flow compressor showing in Figure 3.17. Q-Criterion is used as the method under vortex core region because it is able to analyze three-dimensional vortices. To display a better fluid motion between the tip and compressor casing, velocity vector is placed at the middle of blade. Table 4.4 shows the visualization result of velocity vector as side view of axial flow compressor as in Figure 3.17.

Numerical analysis of result refers to the lift and drag coefficient in Figure 4.1 to 4.3 are the simulation results of fluent. When the solution has achieved constant stable line after certain number of iteration, the lift and drag coefficient is extracted from the graph. Lift coefficient is divided by drag coefficient in order to obtain lift to drag coefficient as shown in Table 4.5.

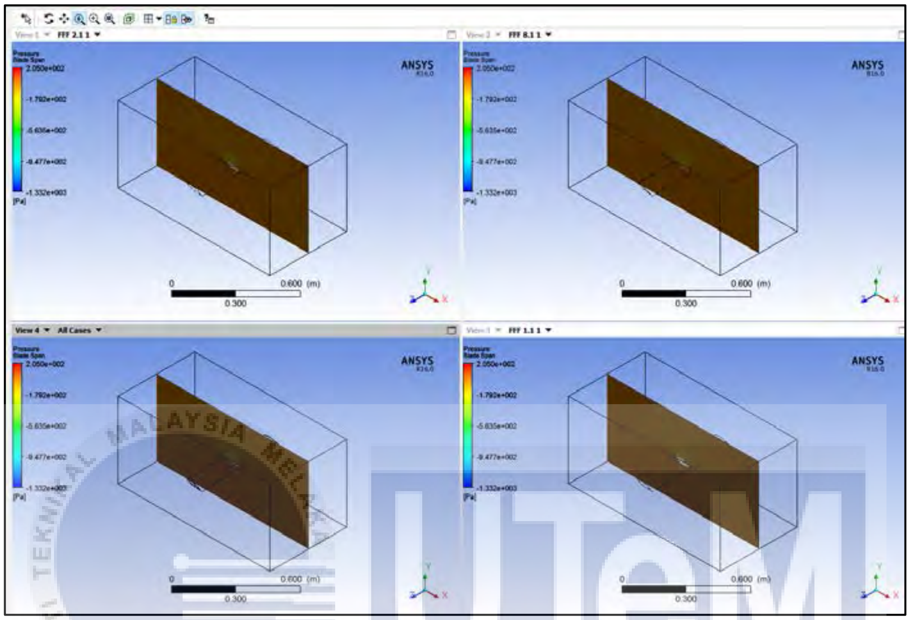

(a)

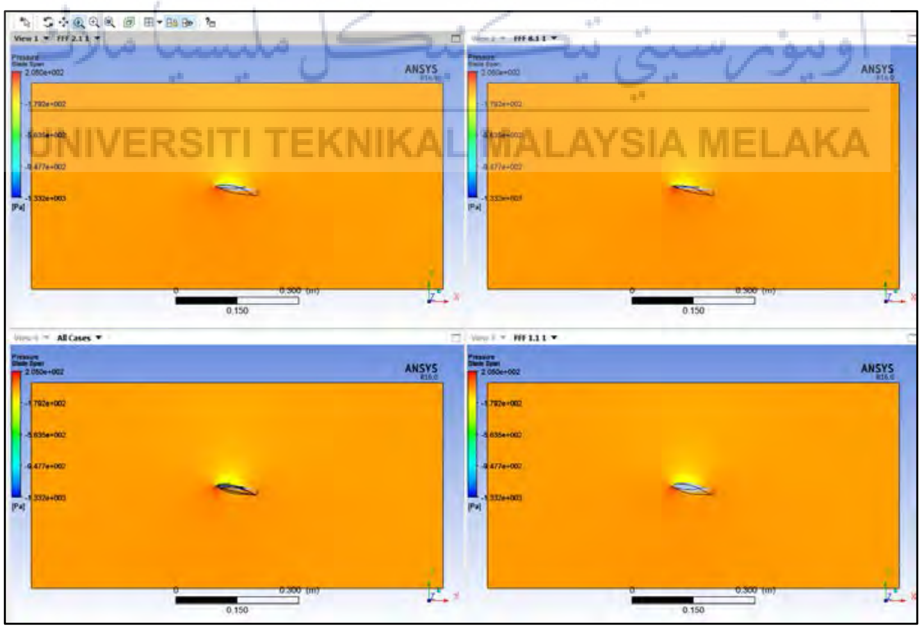

(b)

Figure 3.16(a) Isometric View and (b) Side View of Result Analysis for All Profiles

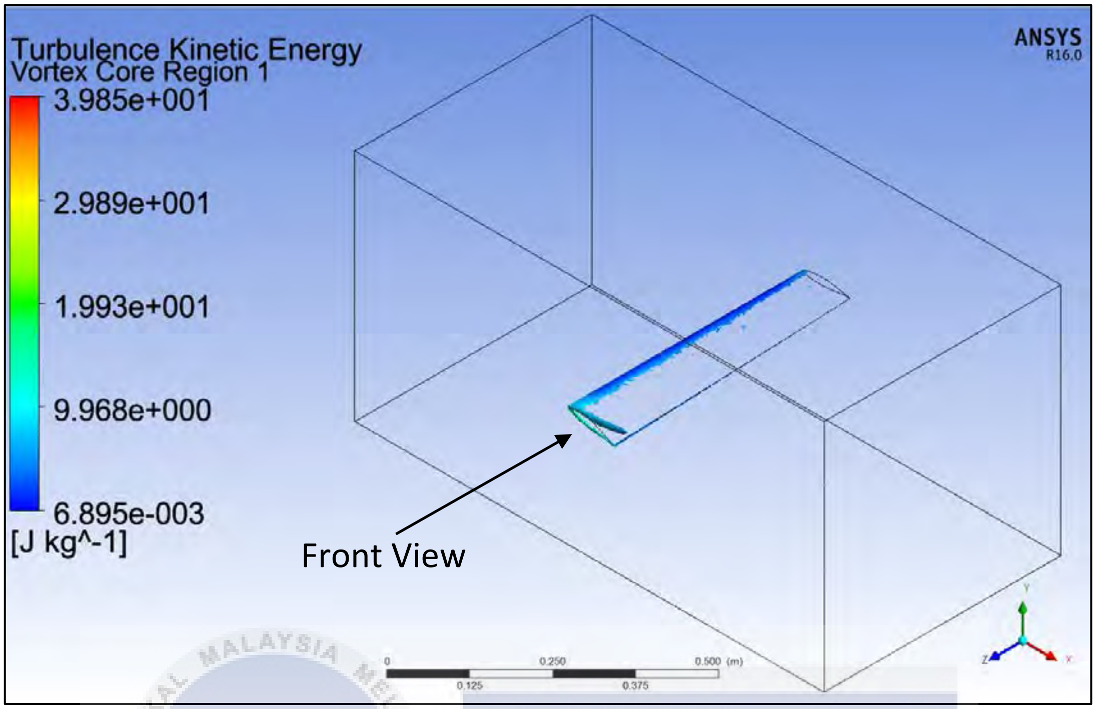

Figure 3.17 Isometric View of Vortex developed due to Tip Leakage of Blade

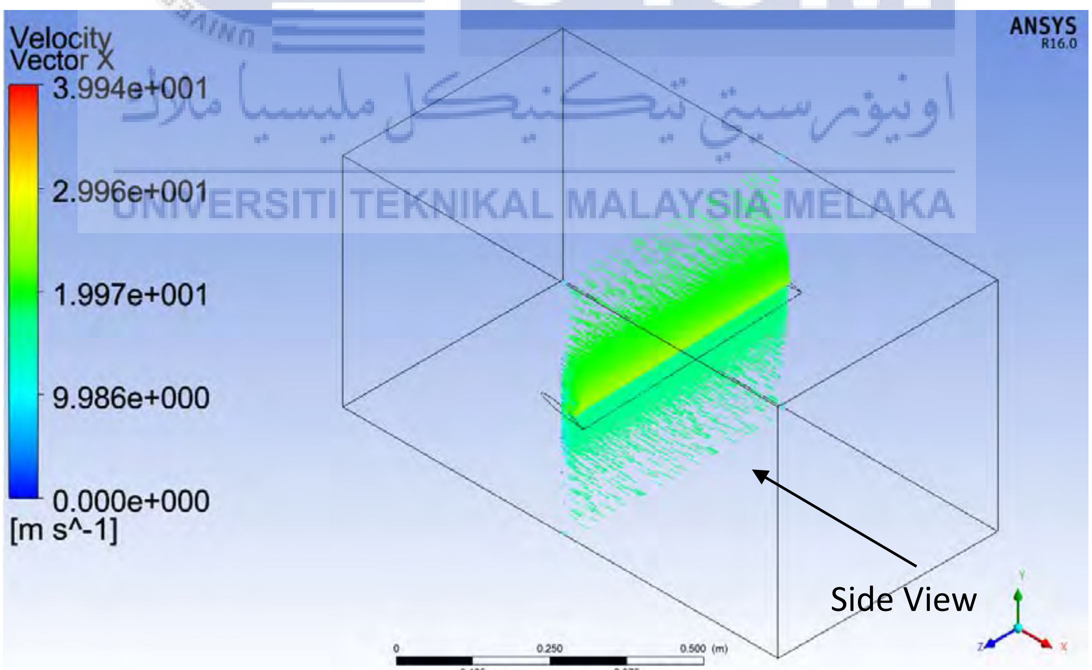

Figure 3.18 Isometric View of Velocity Vector developed due to Tip Leakage of Blade

CHAPTER 4

RESULTS ANALYSIS AND DISCUSSION

This chapter will display the simulation results regarding to pressure contour and velocity vector of blade profiles NACA 65(2)415, NACA 65(410) and NACA 65(4)221. This chapter will also discuss about how the shape and tip clearance of a single profile affecting the performance of an axial flow compressor.

Result analysis of this simulation requires the consideration of a three dimensional twisted blade. The air flowing across the three dimensional twisted blade is varied from the hub to the tip of blade. Twisting angle represents the angle of twist of blade at depending on the segment of blade span. Due to this circumstance, two dimensional views of pressure contour are taken at a specific cross section of blade showing in Table 4.1. To analyze the result efficiently, percentage of blade span is used to describe the length segment of the blade as in Figure 4.1. For example, the target of blade span is 0.05m measured from the root, the percentage of blade span will be 10% since the blade height is 0.5m. The percentage or segment of blade span increases by 0.05m or 10% when going down Table 4.1. From Table 4.2 to 4.2.5, each table displays the results of velocity vector at a specific blade span and twisting angle. The lift and drag coefficient of each profiles are extracted from graph in Figure 4.2 to 4.4 and tabulated in Table 4.5. Figure 4.5 records the lift to drag coefficient of each profiles.

For the case vortex analysis, vortex core region (Q-criterion) is used to observe three-dimensional vortex forming on the suction side of airfoil blades. Table 4.3 displays the tip leakage vortex formed and Table 4.4 shows the fluid motion from the pressure to the suction side of different blade profiles.

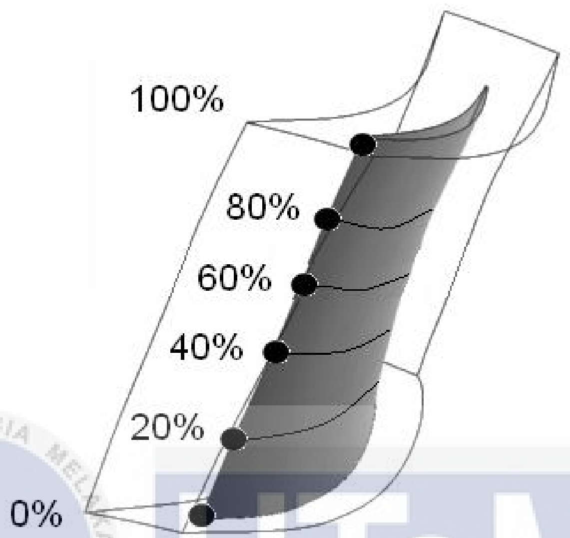

Figure 4.1 Percentage of Blade Span is introduced for the description of Blade Length

Table 4.1: Pressure Contour of NACA 65(2)415, NACA 65(410) and NACA 65(4)221

Blade Span	NACA 65(2)415	NACA 65(410)	NACA 65(4)221
At 10%, $\theta = 1.4°$	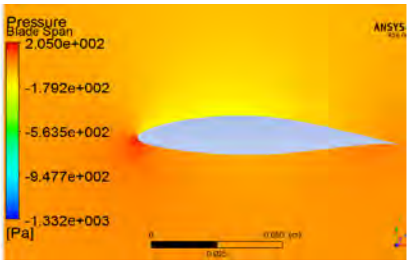	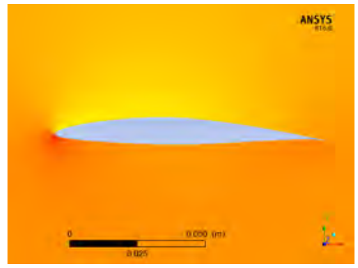	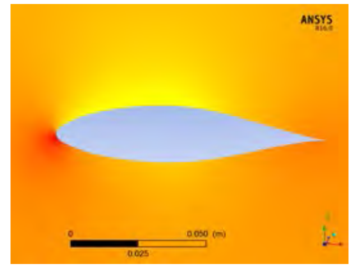
At 20%, $\theta = 2.8°$	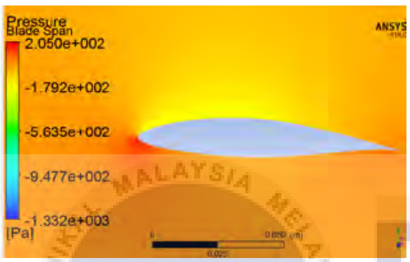	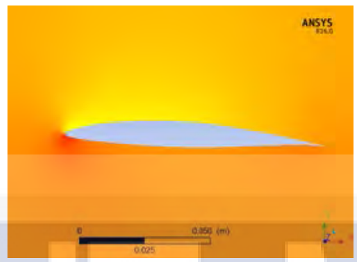	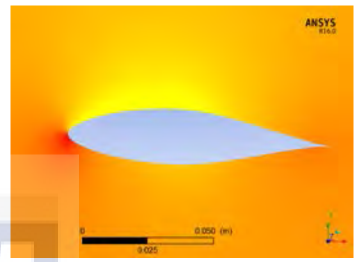
At 30%, $\theta = 4.2°$	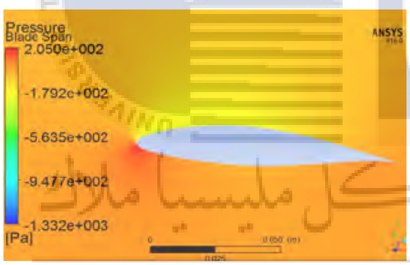		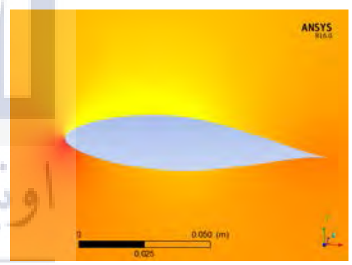
At 40%, $\theta = 5.6°$	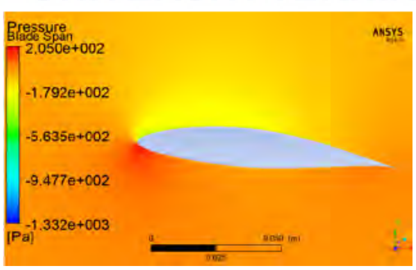	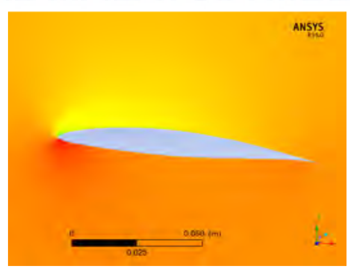	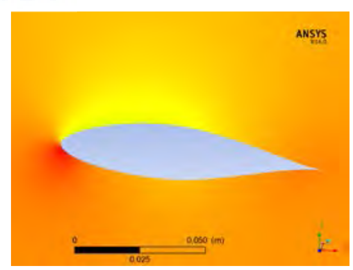
At 50%, $\theta = 7.0°$	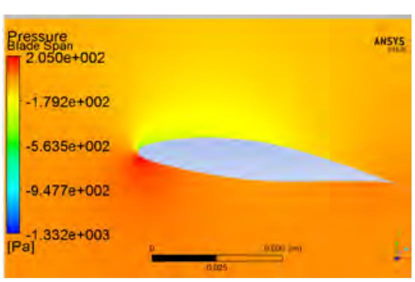	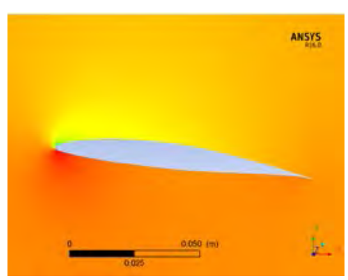	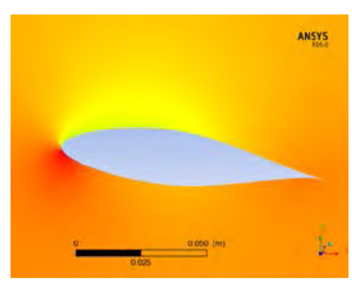

Blade Span	NACA 65(2)415	NACA 65(410)	NACA 65(4)221
At 60%, $\theta = 8.4°$	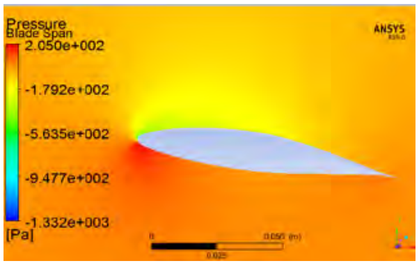	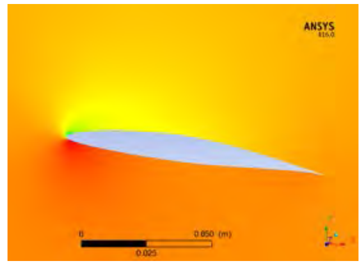	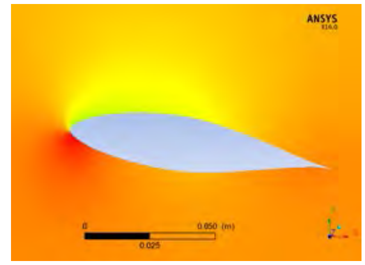
At 70%, $\theta = 9.8°$	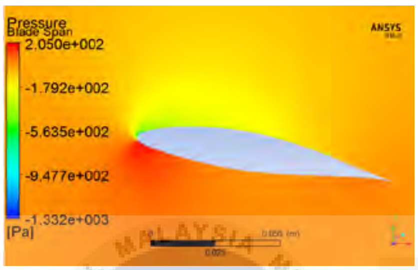	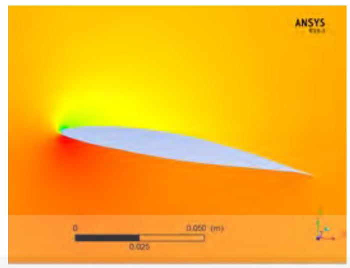	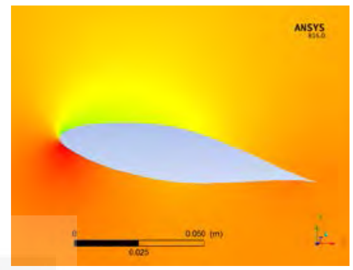
At 80%, $\theta = 11.2°$	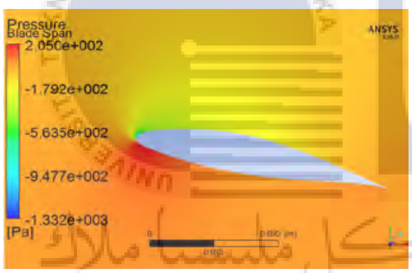		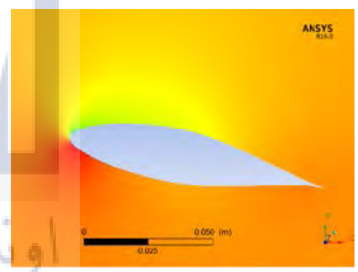
At 90%, $\theta = 12.6°$	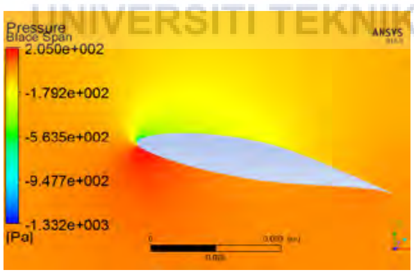	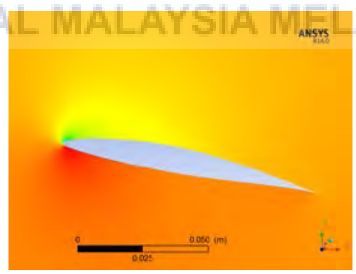	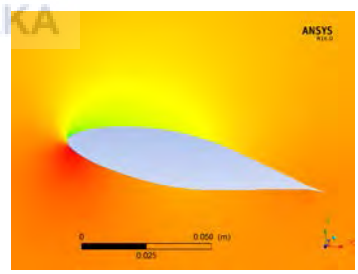
At 99%, $\theta = 13.9°$	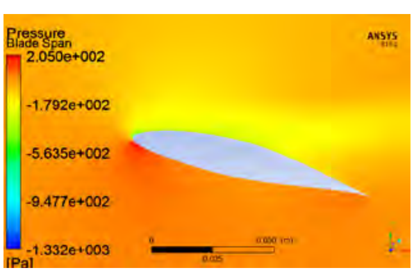	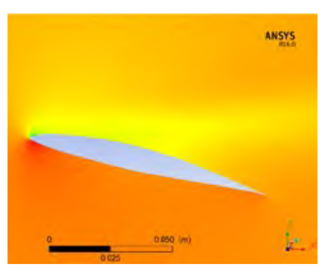	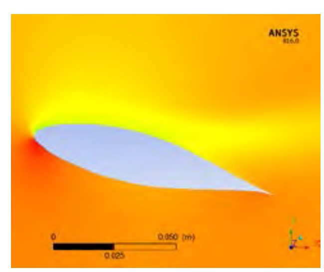

Note: All blade profiles subjected to same pressure legend

Table 4.1 shows the Pressure Contour of NACA 65(2)415, NACA 65(410) and NACA 65(4)221. From blade span 10% to 99%, it is noticeable that blade profile NACA 65(4)221 retains yellowish at the suction side of blade compared to other profiles. This indicates that the velocity at the particular area of NACA 65(4)221 is high, which results in a low pressure region. This activity suggests the lift coefficient of NACA 65(4)221 is only as low as 3.3791 as shown in Table 4.5. On the other hand, the high color contrasts between suction and pressure side of blade profiles NACA 65(2)415 and NACA 65(410) represents both profiles has high lift coefficient due the pressure differences. However, the pressure side of NACA 65(2)415 shows wider yellow region compared to NACA 65(410). This shows the pressure difference between suction and pressure side of profile NACA 65(2)415 is higher than NACA 65(410). High pressure difference between suction and pressure side of profile results in higher lift coefficient which explains that NACA 65(2)415 has the highest lift coefficient of 3.9607.

Table 4.2: Velocity vector of NACA 65(2)415, NACA 65(410) and NACA 65(4)221

Parameter	At blade span 20%, $\theta = 2.8°$
NACA 65(2)415	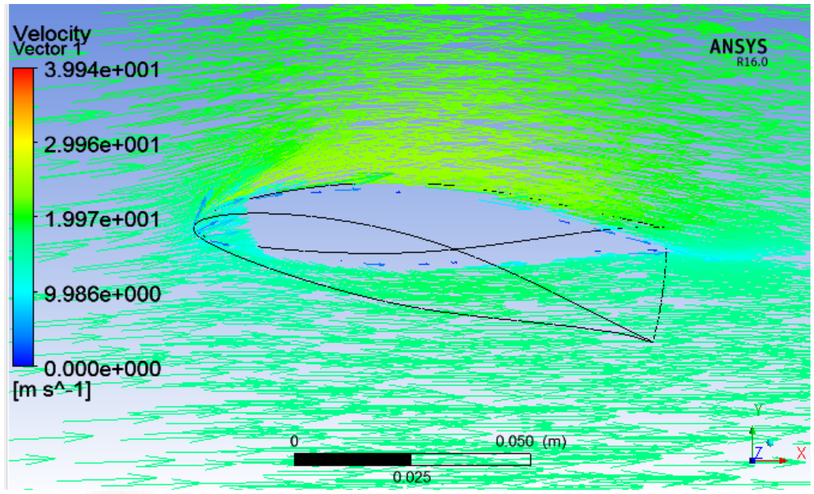
NACA 65(410)	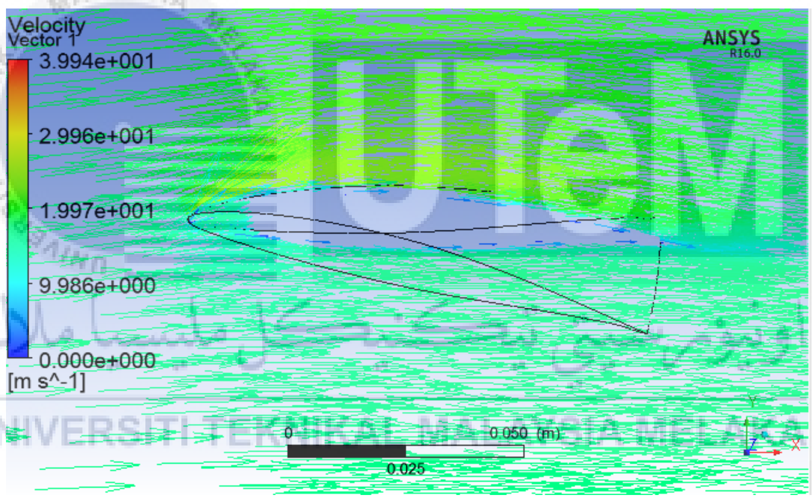
NACA 65(4)212	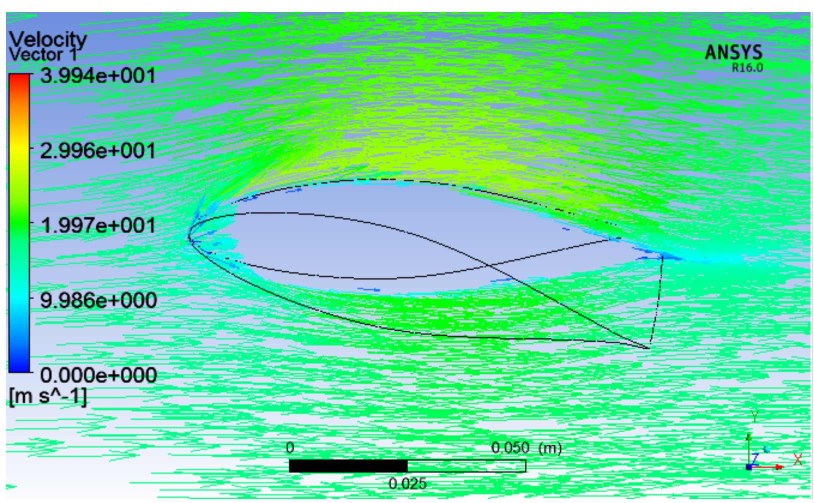

Table 4.2.1: Velocity vector of NACA 65(2)415, NACA 65(410) and NACA 65(4)221

Parameter	At blade span 40%, $\theta = 5.6°$
NACA 65(2)415	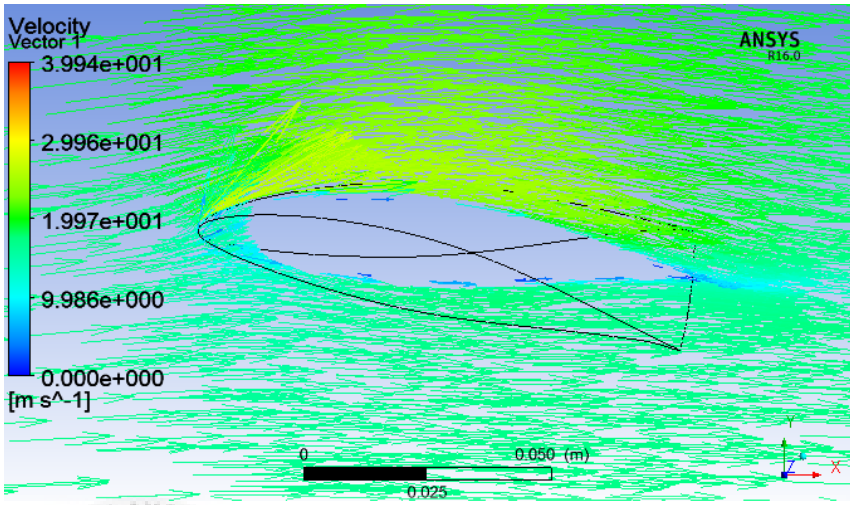
NACA 65(410)	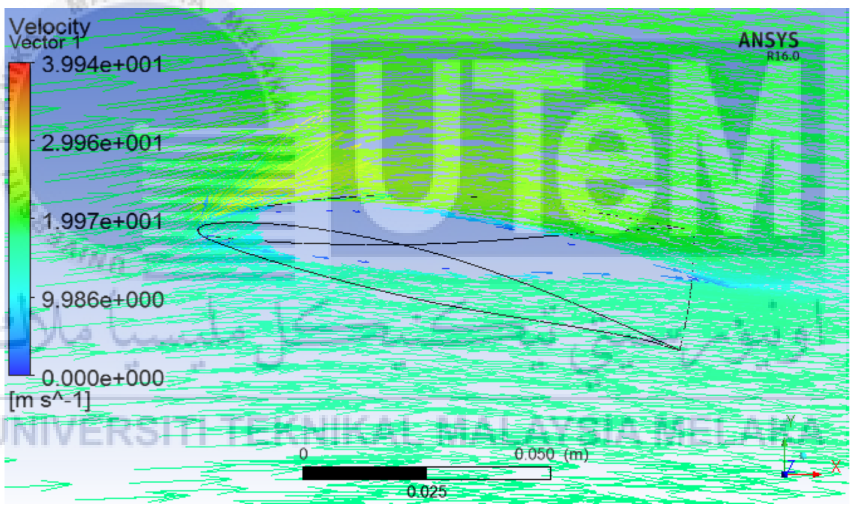
NACA 65(4)221	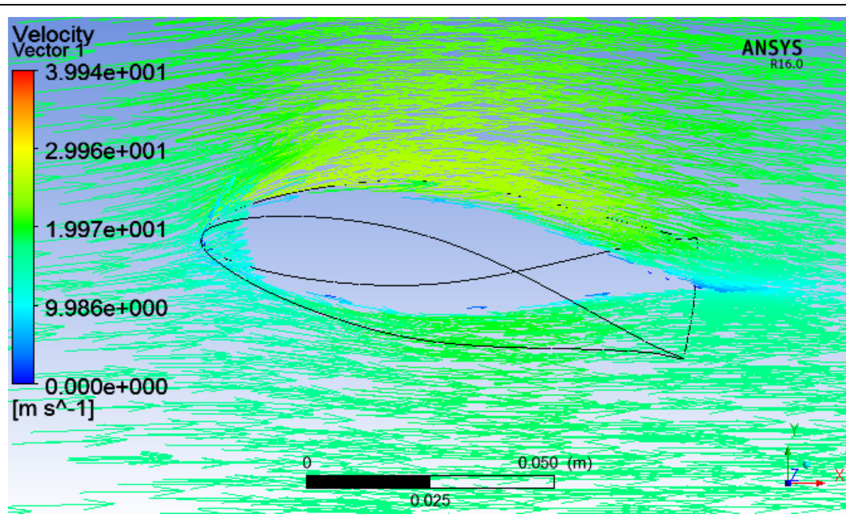

Table 4.2.2: Velocity vector of NACA 65(2)415, NACA 65(410) and NACA 65(4)221

Parameter	At blade span 60%, $\theta = 8.4°$
NACA 65(2)415	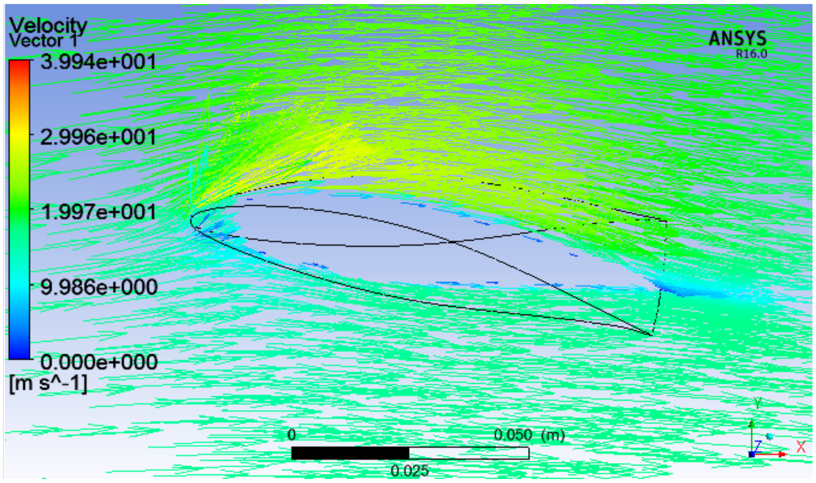
NACA 65(410)	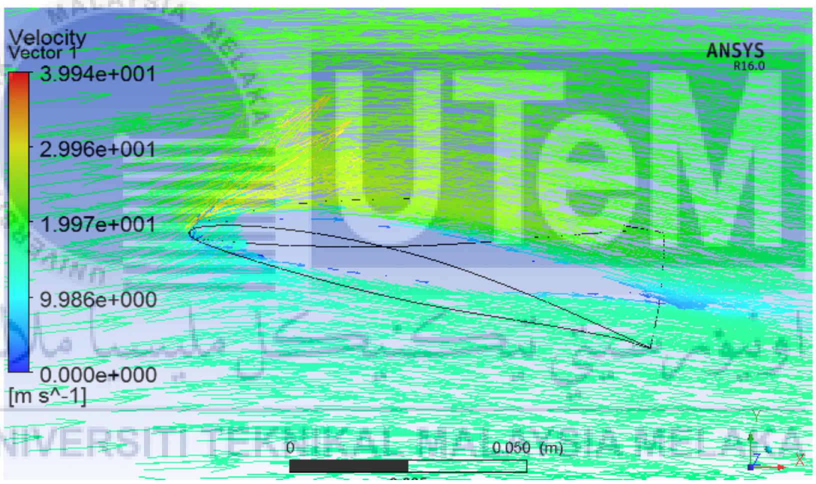
NACA 65(4)221	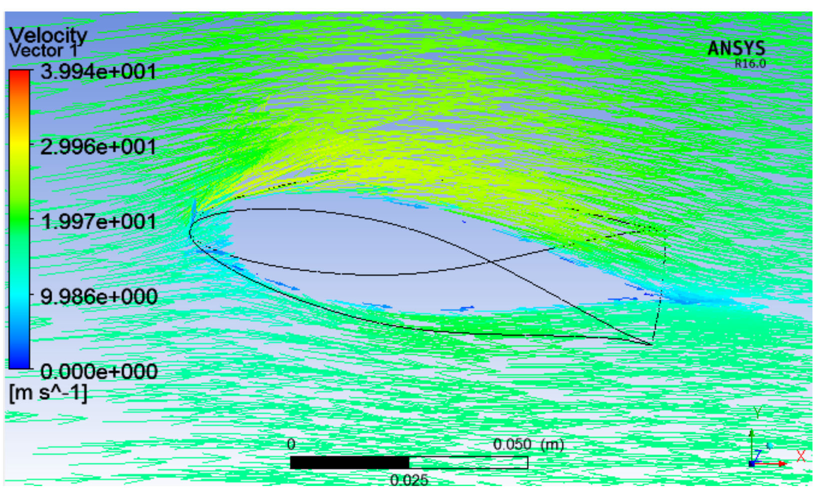

Table 4.2.3: Velocity vector of NACA 65(2)415, NACA 65(410) and NACA 65(4)221

Parameter	At blade span 80%, $\theta = 11.2°$
NACA 65(2)415	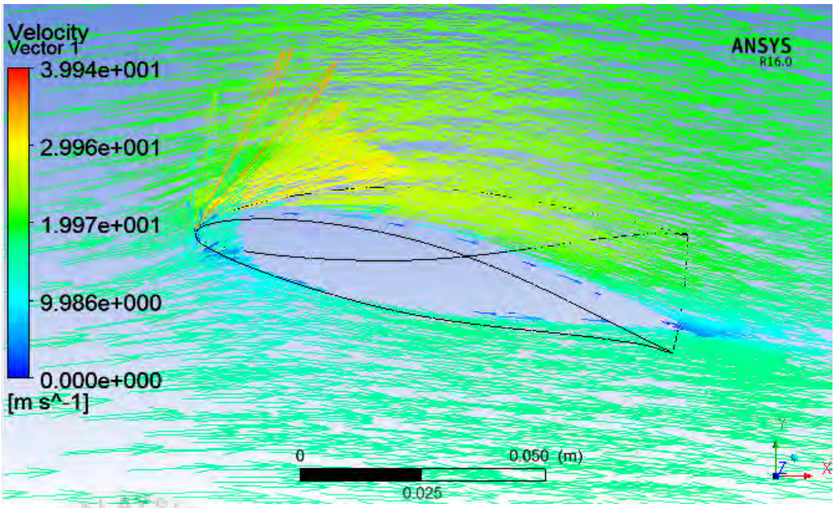
NACA 65(410)	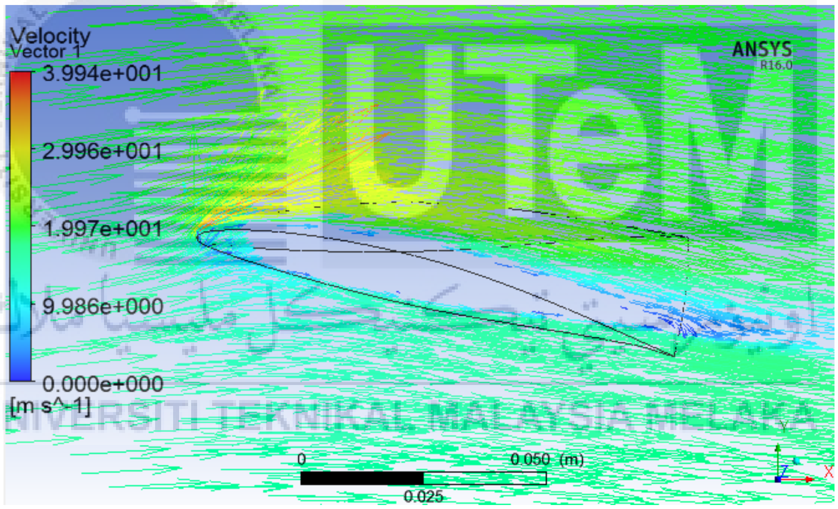
NACA 65(4)221	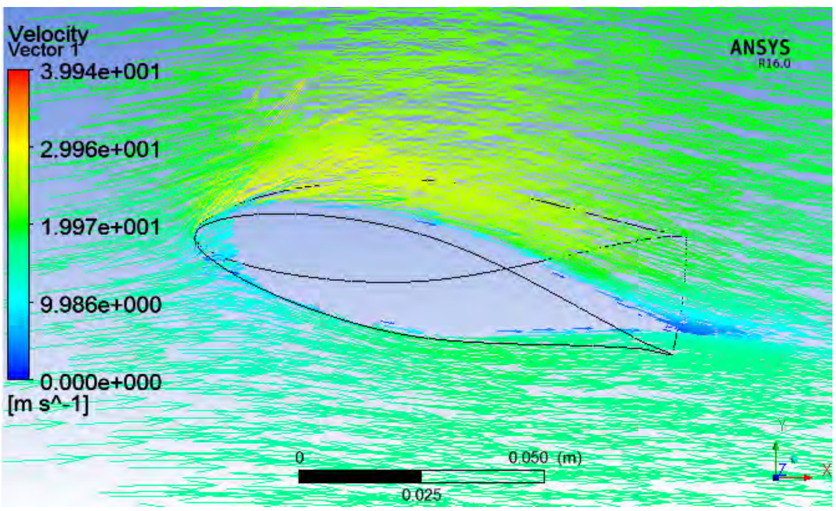

Table 4.2.4: Velocity vector of NACA 65(2)415, NACA 65(410) and NACA 65(4)221

Parameter	At blade span 99%, $\theta = 13.9°$
NACA 65(2)415	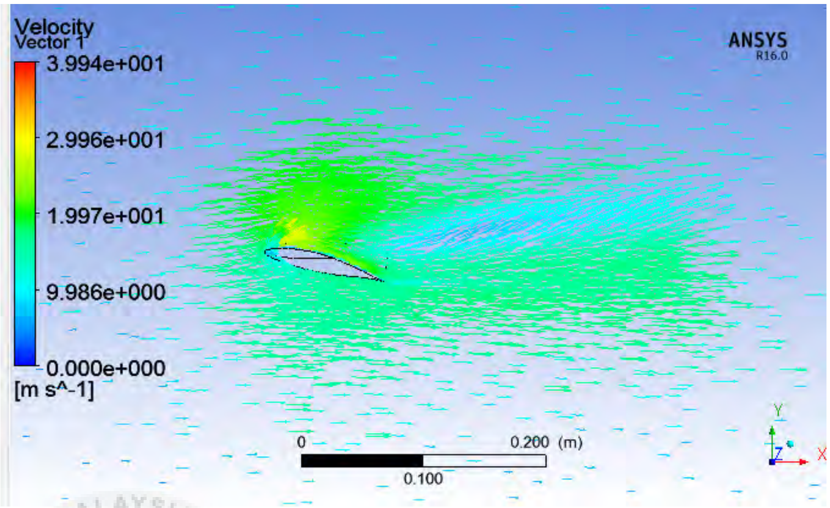
NACA 65(410)	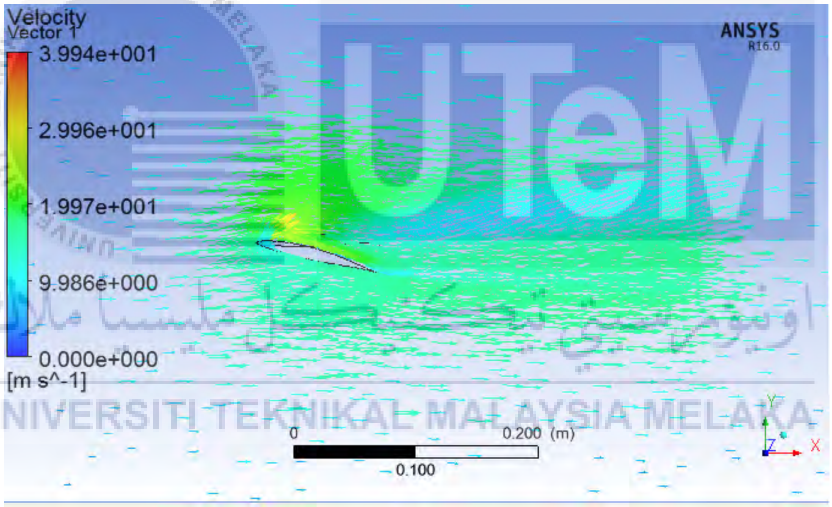
NACA 65(4)221	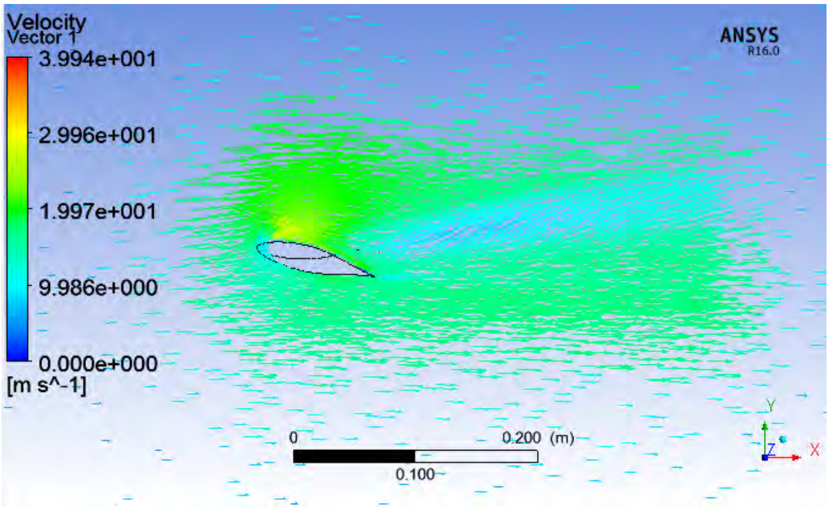

In Table 4.2 to 4.2.4 shows the velocity vector of NACA 65(2)415, NACA 65(410) and NACA 65(4)221 for blade span 20%, 40%, 60%, 80% and 99% respectively. In Table 4.2 and Table 4.2.1, the fluid flow at the trailing edges of all three profiles rejoins well without any separation. In Table 4.2.2, slight blue region is formed at the trailing edge of profiles showing that separation of fluid starting to occur. In Table 4.2.3, all the profiles have enlarged separation region. However, vortex is formed only at the trailing edge of NACA 65(410). This explains that the drag coefficient of NACA 65(410) is higher than other profiles. In Table 4.2.4, the views of profiles are scaled down to observe the tip leakage vortex formed on the suction sides of profiles.

Table 4.3: Tip Leakage Vortices (Q-Criterion) of various profiles

Profiles	Vortex Core Region, (Q-Criterion)
NACA 65(2)415	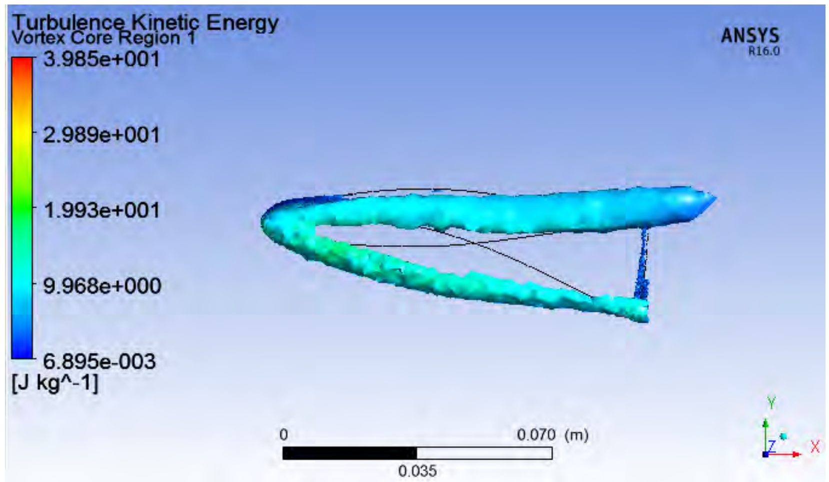
NACA 65(410)	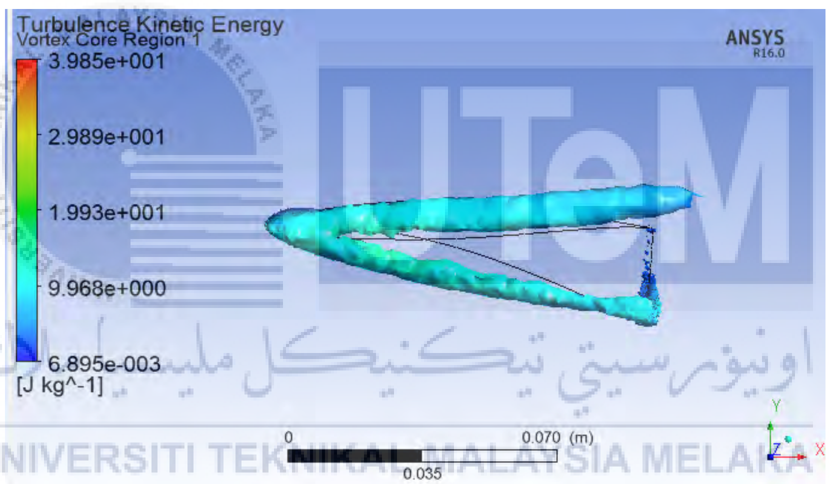
NACA 65(4)221	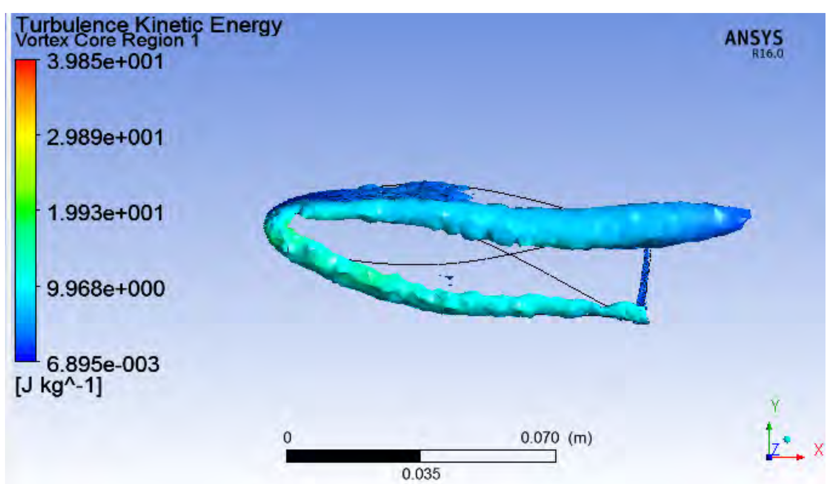

Table 4.4: Tip Leakage Vortices Velocity Vector of various profiles

Profiles	Velocity Vector
NACA 65(2)415	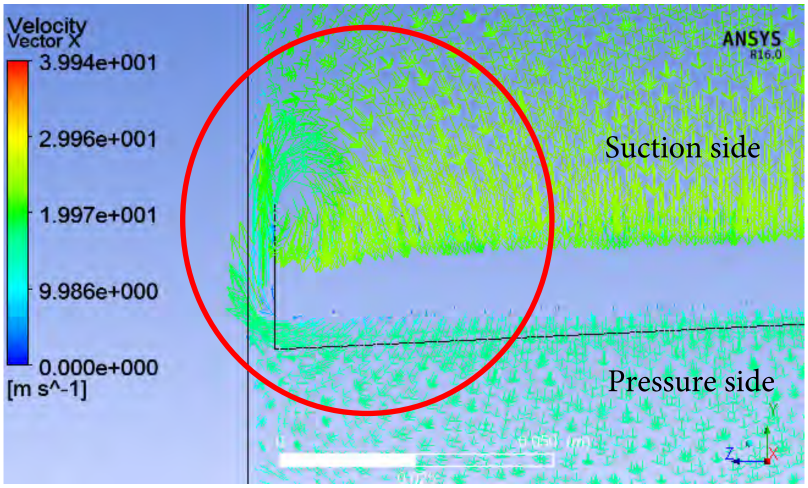
NACA 65(410)	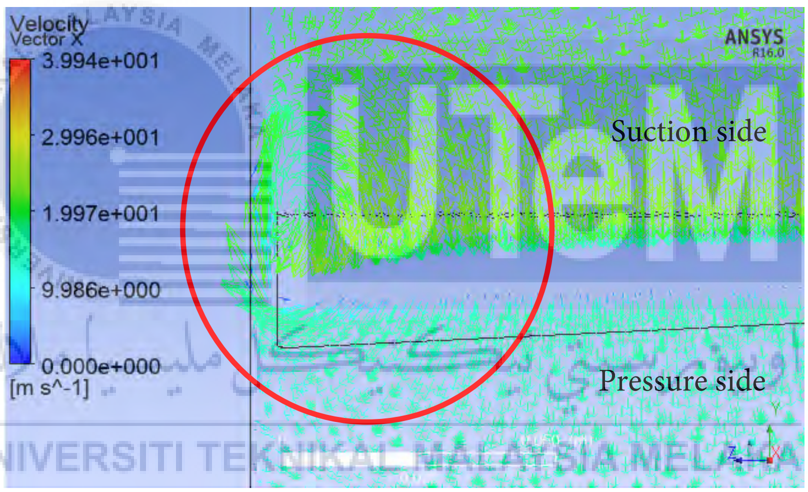
NACA 65(4)221	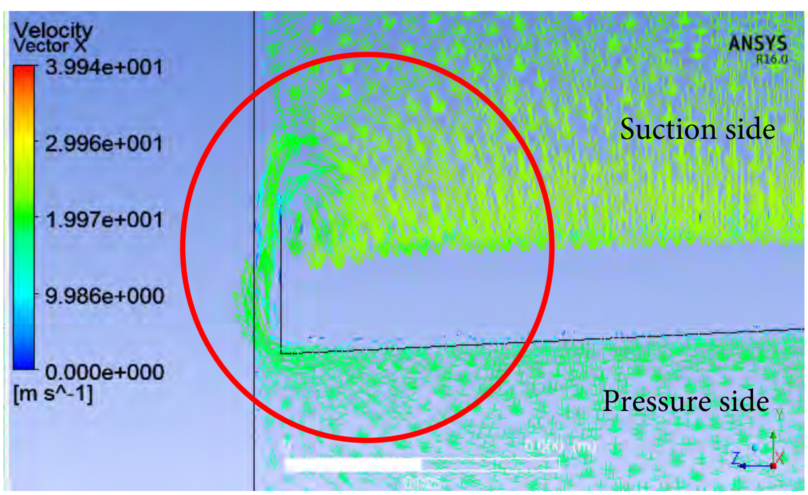

Table 4.3 shows the tip leakage vortex formed on the suction side of NACA 65(2)415, NACA 65(410) and NACA 65(4)221. Vortices are observed by creating vortex core region (Q-Criterion) under iso-surface of result post-processing. It can be seen that the vortex formed on the suction side of NACA 65(4)221 has the lowest volume and turbulence kinetic energy followed by NACA 65(2)415 and NACA 65(410). This study shows that during the rotation of blade, the vortex formed in NACA 65(4)221 is less likely to resist the rotation of compressor blade. In Table 4.4, tip leakage vortex is shown in the form of velocity vector. The velocity on the suction side of blade is lower compared to pressure side of blades. This result in high pressure difference between both sides and air tends to slip through the tiny clearance between the compressor's casing wall and blade tip. Due to the non-slip condition of blade and casing wall, a highly turning flow are shaped on suction side of blade.

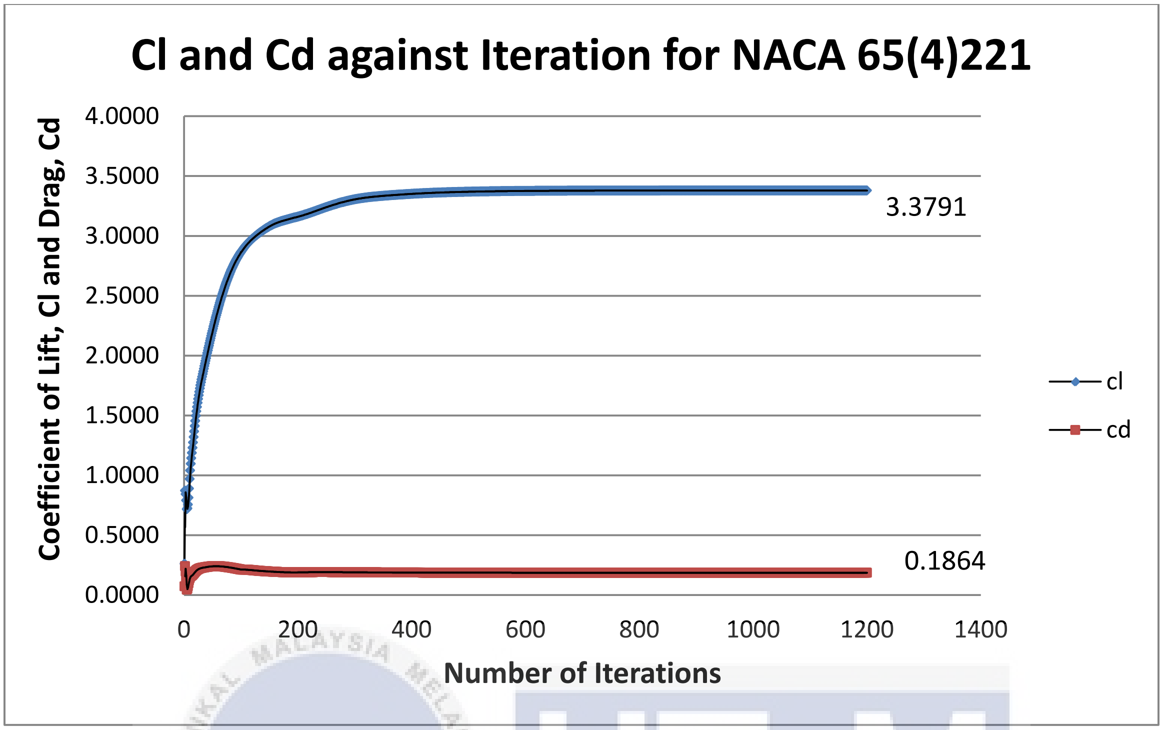

Figure 4.2 Coefficient of Lift and Drag against Number of Iterations for NACA 65(4)221

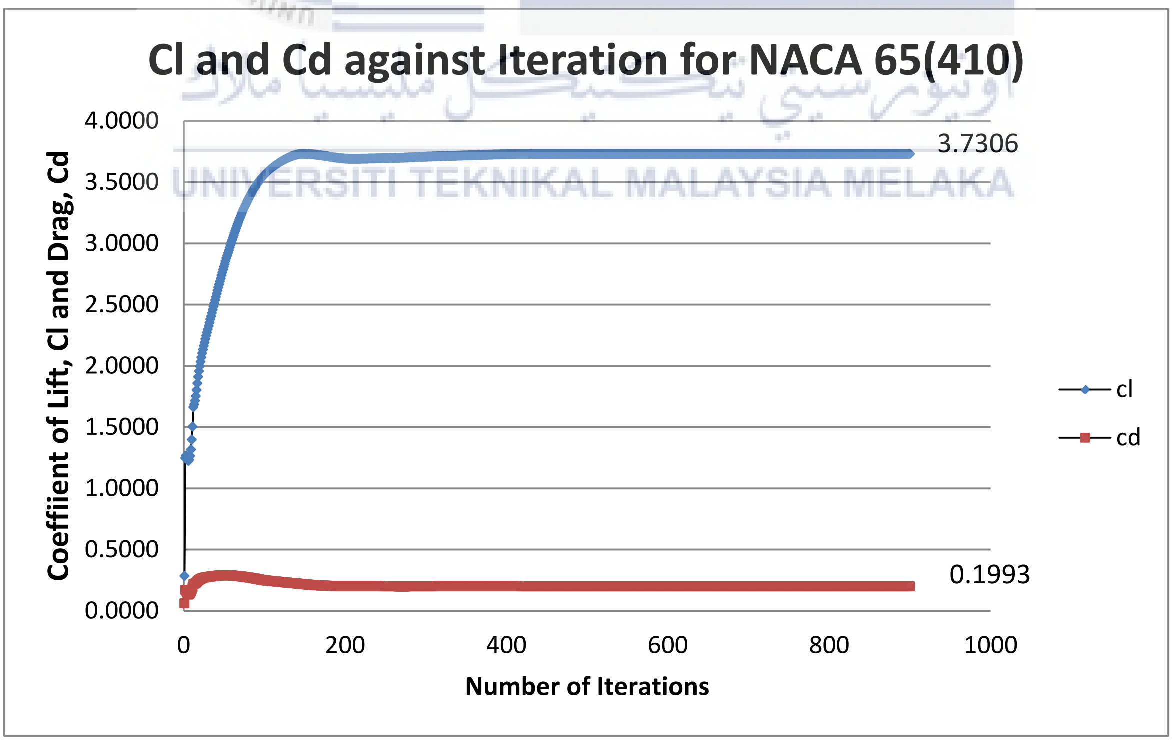

Figure 4.3 Coefficient of Lift and Drag against Number of Iterations for NACA 65(410)

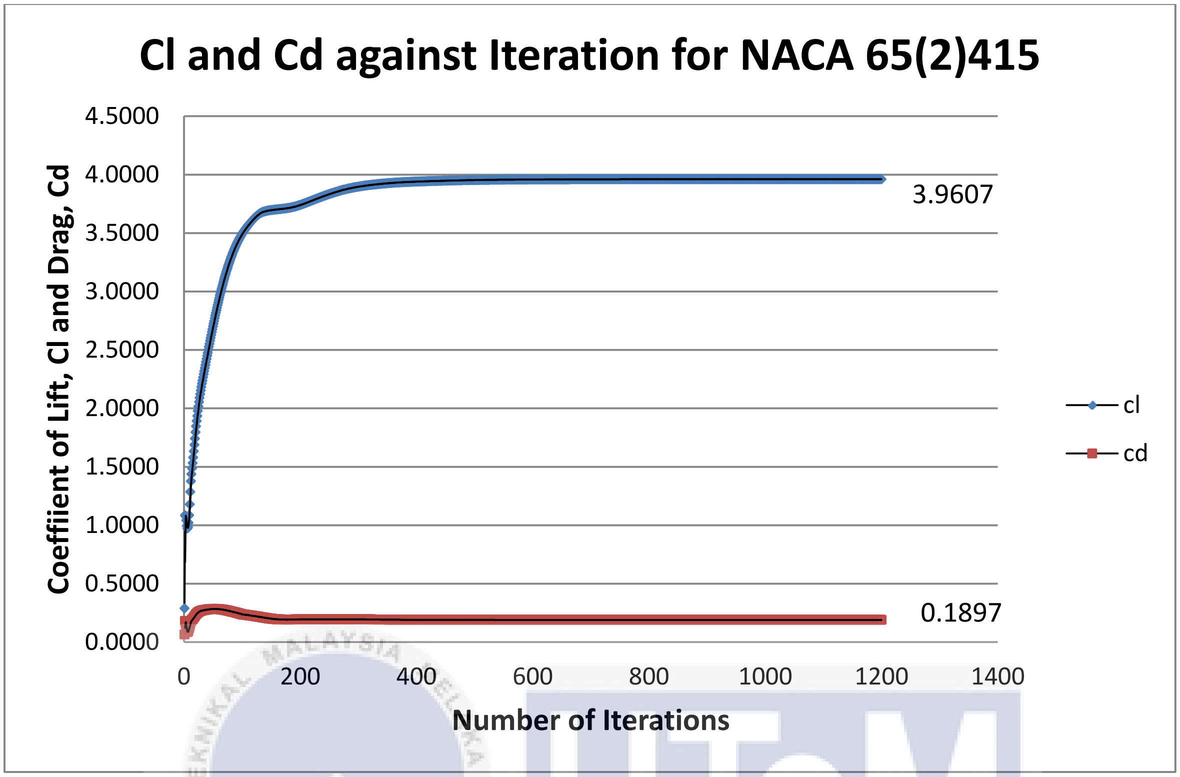

Figure 4.4 Coefficient of Lift and Drag against Number of Iterations for NACA 65(2)415

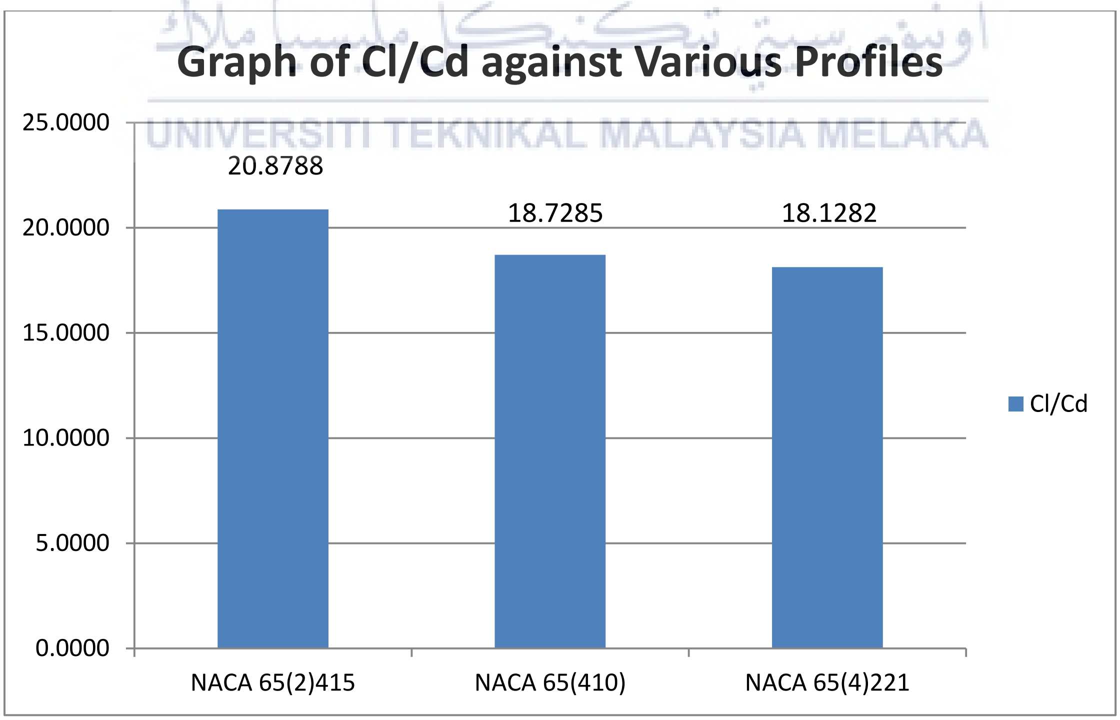

Figure 4.5 Graph of Lift to Drag Coefficient for Various Blade Profiles

Figure 4.2 to 4.3 shows the results of numerical simulation of lift and drag coefficient for profiles NACA 65(2)415, NACA 65(410) and NACA 65(4)221. Since the simulation used in this study is steady flow, the lift and drag coefficient let to be ran until the graph achieves constant zero gradient. In Figure 4.2, lift coefficient achieves constant zero gradient at 3.3791 while drag coefficient achieves constant zero gradient at 0.1864 for profile NACA 65(4)221. In Figure 4.3, lift and drag coefficient that achieves constant zero gradients are 3.7306 and 0.1993 respectively for profile NACA 65(410). In Figure 4.4, lift and drag coefficient that achieves constant zero gradients are 3.9607 and 0.1897 respectively for profile NACA 65(2)415. This values are tabulated in Table 4.5 and simplified to a graph lift to drag coefficient as shown in Figure 4.5.

Table 4.5: Lift, Drag and Lift to Drag Coefficient with respect to Studied Blade Profiles

Blade Profile	Lift Coefficient, Cl	Drag Coefficient, Cd	Lift to Drag Coefficient, Cl/Cd
NACA 65(2)415	3.9607	0.1897	20.8788
NACA 65(410)	3.7306	0.1993	18.7285
NACA 65(4)221	3.3791	0.1864	18.1282

4.2 Lift and Drag Coefficient

Based on the simulation results in Table 4.5, NACA 65(2)415 has the highest lift to drag coefficient of 20.8788. From the pressure contour of NACA 65(2)415 and NACA 65(410) in Table 4.1, both profiles has lift coefficient of 3.9607 and 3.7306 respectively. The high color contrast above and below these blade indicates that the pressure difference is high enough to generate lift force and ultimately contributes to lift coefficient of these profiles. However, for the blade profile NACA 65(4)221, it has slight yellowish and the bottom region of its region which lowers the lift force acted on the blade, leading to the drop of lift coefficient to 3.3791.

Data in Table 4.5 suggests that NACA 65(410) has the highest drag coefficient. Based on the visualization of velocity profiles in Table 4.2, the color of velocity arrows above all the profiles are yellowish while the color shows greenish at bottom of the blade. This phenomenon explains the situation of Bernoulli's Principle where the fluid flow above a streamlined body is faster compared to its bottom which results in lift force on a blade. The fluid rejoins well after flowing across the blades but separation region starts to develop as the twist angle of the blades increases. In Table 4.2.3, blue separation regions are developed at the trailing edge of blade span 80% and twist angle of 11.2˚. Vortex is formed at the trailing edge of NACA 65(410) which explains the higher drag coefficient compared to other profiles. Vortex formed causes a low pressure region at the trailing end of blade. The pressure at leading edge suppresses the pressure and the trailing edge which contributes to the drag coefficient, as high as 0.1993. Separation region still occurs for the profiles NACA 65(2)415 and NACA 65 (4)221. However, there are no vortices but separations are formed at the trailing edge for both profiles, which lower the values of drag coefficient to 0.1897 and 0.1864 respectively.

4.3 Tip Leakage Vortex

Tip clearance is the minimum gap to prevent any physical contact between a compressor rotor and compressor casing. In this study, the tip clearance is set as 1% of the blade span to investigate the effect of tip leakage flow to the performance of a compressor gas turbine.

Vortex are formed due to the large pressure difference of the pressure and suction side of an airfoil blade. The air flow accelerates through the tiny clearance at the blade tip and swirls on top of the blade as shown in Table 4.4. The casing wall and blade tip both are non-slip wall, the viscosity of these wall results in friction when air flowing through the gap. This eventually forms a highly turning vortex on the suction side of blade.The red highlighted area represents the vortex formed at the suction side of NACA 65(2)415, NACA 65(410) and NACA 65(4)221. Table 4.3 shows the three dimensional view of vortices formed on suction sides of blade profiles. Based on colour visualization, the vortex formed on NACA 65(410) profiles has the highest turbulence kinetic energy followed by NACA 65(2)415 and NACA 65(4)221. Table 4.2.4 also shows the vortices in the form of white and blueish region. These vortices are detrimental to the performance of compressor in term of pressure rise and efficiency. The vortices formed at suction side of blade creates a barrier to the rotating compressor rotor that might cause the reduction in blade rotational speed and instability. This ultimately cause the reduction in pressure at the exit of compressor and reduction of efficiency.

CHAPTER 5

CONCLUSION AND RECOMMENDATION

Lift to drag ratio and tip leakage vortex are the two criteria affecting the performance of compressor in this study. Based on the discussion in Chapter 4, NACA 65(2)415 has the highest lift to drag ratio of 20.9. This indicates that NACA 65(2)415 is able to generate great thrust force and low drag force, minimize the load of compressor and thus increase the efficiency of compressor. NACA 65(410) and NACA 65(4)221 both has a lift to drag ratio of 18.7 and 18.1 repectively. However, the tip leakage is the other contributing factor to the compressor performance. NACA 65(4)221 is suggested as the lowest impact in term of tip leakage vortex followed by NACA 65(2)415 and NACA 65(410). The blockage effect due to vortex formed at the suction side 65(4)221 is the lowest, marks to reduce the rotational torque required for the spinning of compressor blade. This concludes that NACA 65(2)415 is the most suitable blade profile for the performance of compressor in term of lift to drag coefficient but not until the situation of tip leakage vortex is able to control. Further investigation shall be made in which lift to drag ratio or tip leakage vortex would be the main contributing factor to the performance of compressor for its pressure rise and efficiency. The method of tip leakage vortex reduction such as active control actuator and tip rounding for NACA 65(2)415 shall also be studied to improvise this rotor blade for better performance.

REFERENCES

Andersson, B., Andersson, R., Hakansson, L., Mortensen, M., Sudiyo, R., Wachem, B.V. (2012).Computational Fluid Dynamics for Engineers. New York, America.

Azad, G., Je-Chin, Han., Shuye, T. (2000). Heat Transfer and Pressure Distribution on a Gas Turbine Blade Tip. *Journal of Turbomachinery*. 122(4), pp 725-732.

Balje, O.E. (1964). A Study of Reynolds Number Effects in Turbomachinery, *Journal of Engineering for Power*, ASME Trans., 86(3), pp 227-235.

Bindon, J.P., 1989. The measurement and formation of tip clearance loss. ASME Journal of Turbomachinery, 111, pp 258-263

Boyce, M.P. (2012). Gas Turbine Handbook (4th Edition), Houston, Texas, Ameria.

Brun, K., Kurz, R. (2001). Aerodynamic Instability and Life Limiting Effects of Inlet and Interstage Water Injection into Gas Turbines and Power. (123), pp 62-69.

Cengel, Y.A., Cimbala, J.M. (2014).Fluid Mechanics Fundamentals and Applications. (Third Edition) . New York, America.

Crivellini, A., Alessandro, V.D., Benedetto, D.D., Montelpare, S., Ricci, R. (2013). Study of laminar separation bubble on low Reynolds number operating airfoils: RANS modelling by means of an high-accuracy solver and experimental verification. *Journal of Physics*. pp 1-13.

Durbin, P.A., Medic, G. (2007). Fluid Dynamics with a Computational Perspective. New York, America.

Giridhar,J., RobertC.M., Katherine, E., Grover A.B., Seyed. S. (2012). Control of Tip-Clearance Flow in a Low Speed Axial Compressor Rotor with Plasma Actuation. *Journal of Turbomachinery*. Vol. 134, pp. 1-9.

Herrig, L.J., Emery, J.C., Erwin, J.R. and Felix, A.R. (1957).Two Dimensional Cascade Tests of NACA 65 series compressor blades at low speeds.National Advisory Committee for Aeronautics. pp. 713-797.

Hunt, R. (2011). The History of the Industrial Gas Turbine.Morpeth, United Kingdom.

Ishizuka, T., Muto, Y., Aritomi, M., Tsuzuki, N. and Kikura, H. (2010).Design and Analysis of an Axial Bypass Compressor Blade in a Supercritical CO_2 Gas Turbine.

Jain, S., Sitaram, N., and Krishnaswamy, S. (2015). Effect of Reynolds Number on Aerodynamics of Airfoil with Gurney Flap. pp. 1-10.

Lampart, P. (2006). Tip Leakage Flows in Turbines. Vol. 2, pp. 139-175.

Lian, Y.S., Shyy, W.(2006). Laminar-Turbulent Transition of a Low Reynolds Number Rigid or Flexible Airfoil. pp 1-25.

Khalid, S.A. (1995). The Effects of Tip Clearance on Axial Compressor Pressure Rise. PhD Thesis, Massachusetts Institute of Technology.

Marusic, I., Joseph, D.D. and Manesh, K.(2007). Laminar and turbulent comparisons for channel flow and flow control. Journal of Fluid Mechanics. Vol. 570, pp. 467-477.

Newbauer, S., Kumpaty, S. (2012).Computational Fluid Dynamics of Aerodynamics Effects for Optimum Number of Wind Turbine Blades. pp. 1-7.

Panigrahi, D.C., Mishra, D.P. (2014).Simulations for the Selection of an Appropriate Blade Profile for Improving Energy Efficiency in Axial Flow Mine Ventilation Fans.Journal of Sustainable Mining. Vol. 13(1), pp. 15-21.

Patel, T.B., Patel, S.T., D.T. Patel,Bhensdadiya, M. (2015). An Analysis of Lift and Drag Forces of NACA Airfoils Using Python.*International Journal of Application or Innovation in Engineering & Management (IJAIEM)*. Vol. (4), pp. 198-206.

Patil, B.S., Thakare, H.R. (2015). Computational Fluid Dynamics Analysis of Wind Turbine Blade at Various Angle of Attack and Different Reynolds Number. *International Conference on Computational Heat and Mass Transfer*. Vol. (127), pp. 1363-1369.

Roland, A., Galison, P. (2000). Atmospheric Flight in the Twentieth Century. United Kingdom.

Sanchez, S.J.R. (2014). Analysis of Flow Separation over Aerodynamics Airfoils.Universidad Carlos III de Madrid, Spain.

Versteeg, H., Malalasekera, W. (2007). An Introduction to Computational Fluid Dynamics:The Finite Volume Method. (Second Edition). New York, America.

Yusof, A., Wasbari, F., Saadun, N.A., Zakaria, S. (2014). Fluid Power System, Introduction to Fluid Power System. Melaka, Malaysia.

Airfoil characteristics.(2009) Retrieved from http://www.airspace.cz/akademie/rocnik/2009/12/airfoils.php

Using Flow Boundary Conditions. (2006, September 20).Retrieved from https://www.sharcnet.ca/Software/Fluent6/html/ug/node216.htm

Figure 1.1 The principle behind an airfoil blade. Retrieved from https://naturalistsmiscellany.files.wordpress.com/2012/07/flight-mechanics-lift1.jpg, by H.Hinam.

Figure 4.1. Aerodynamic optimisation of NASA rotor 37 compressor rotor blade. Retrieved from https://hygprogramming.wordpress.com/industrial-applications/aerodynamic-optimisation-of-nasa-rotor-37-compressor-rotor-blade/

LIST OF APPENDICES

Appendix A: Project Timeline Gantt Chart for PSM I &II

PSM I

Activities	Week														
	01	02	03	04	05	06	07	08	09	10	11	12	13	14	15
Briefing and planning	■														
Meeting with Supervisor		■	■												
Literature review		■	■	■	■	■	■	■	■	■	■	■	■		
Profile Drawing				■	■	■	■	■							
Introduction				■	■	■									
Methodology							■	■	■						
PSM I final report		■	■	■	■	■	■	■	■	■	■	■	■	■	
Seminar I															■

PSM II

Activities	Week														
	01	02	03	04	05	06	07	08	09	10	11	12	13	14	15
Briefing and planning	■														
Literature review		■	■	■	■										
Wind Tunnel Drawing			■	■	■	■	■								
CFD Simulation						■	■	■	■	■	■				
Result Analysis									■	■	■	■			
Discussion												■	■		
Seminar Presentation													■	■	
Correction Report														■	■
Final Report Submission															■

Appendix B: Drawing for Blade Profile NACA 65(2)415

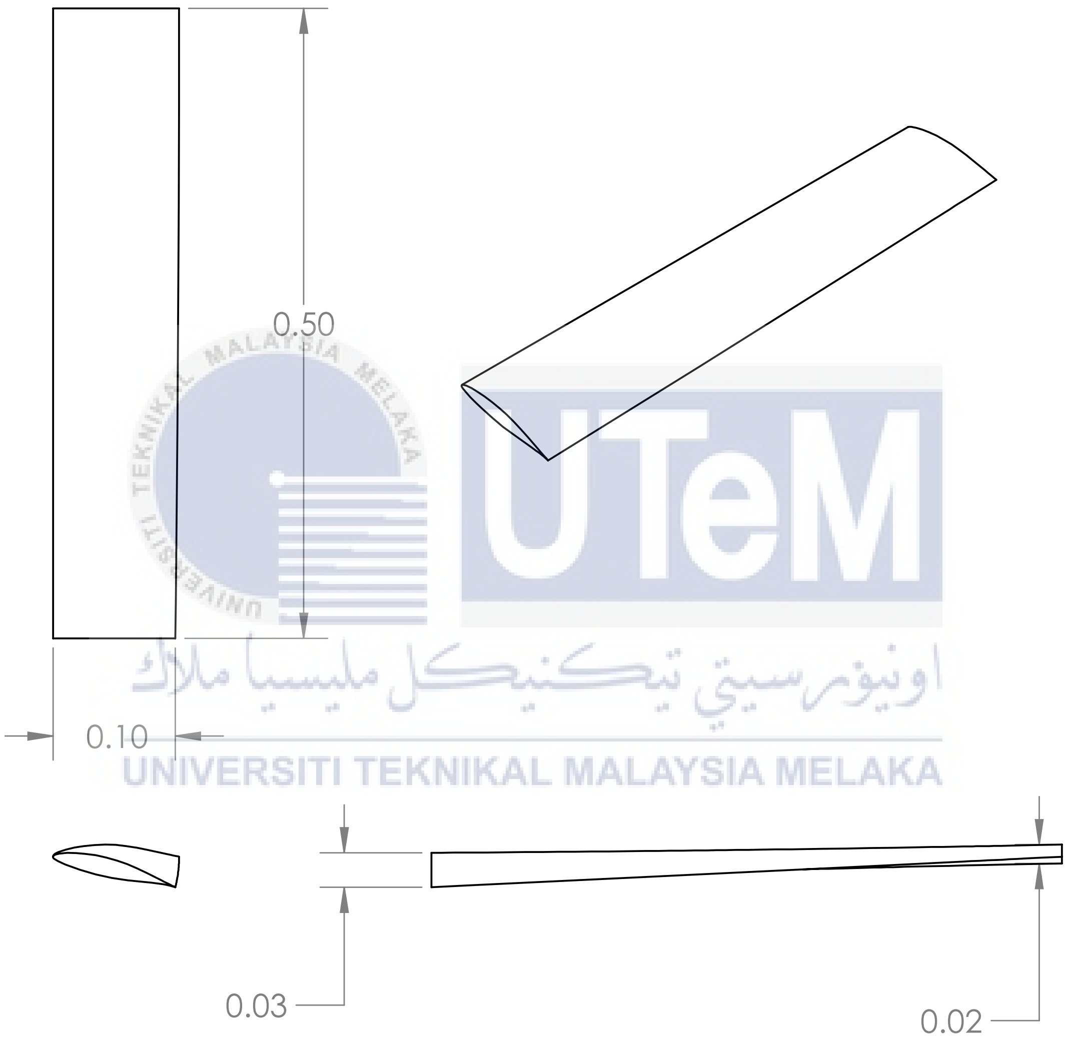

UNLESS OTHERWISE SPECIFIED: DIMENSIONS ARE IN MILLIMETERS SURFACE FINISH: TOLERANCES: LINEAR: ANGULAR:	FINISH:	DEBURR AND BREAK SHARP EDGES	DO NOT SCALE DRAWING — REVISION FINAL YEAR PROJECT 2017

	NAME	SIGNATURE	DATE
DRAWN			
CHK'D			
APPV'D			
MFG			
Q.A			

TITLE:

BLADE PROFILE
NACA 65(2)415

MATERIAL:

DWG NO.

UNIT: Metre

A4

WEIGHT:

SCALE:1:8

SHEET 1 OF 1

Appendix C: Drawing for Blade Profile NACA 65(4)221

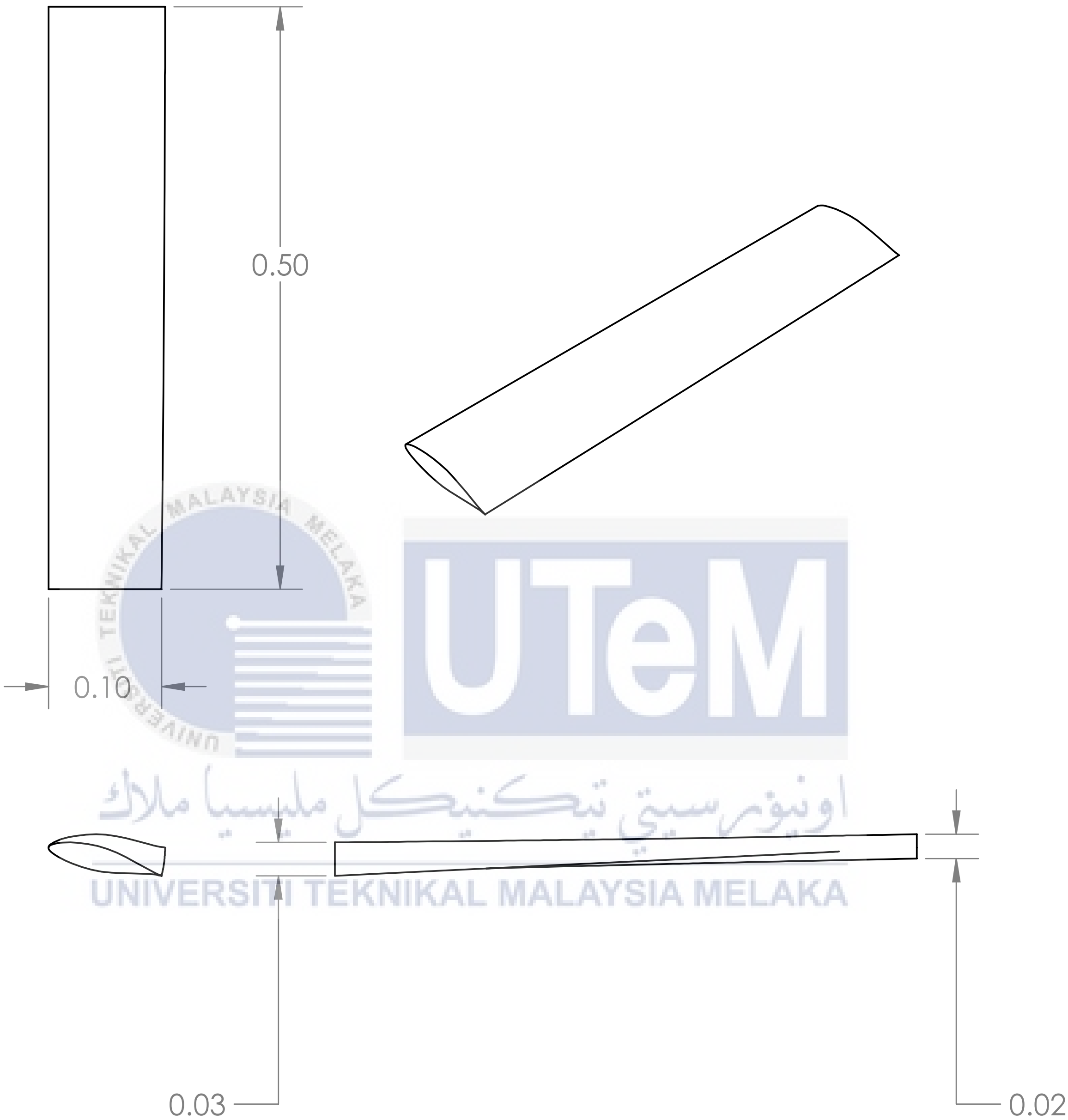

UNLESS OTHERWISE SPECIFIED: DIMENSIONS ARE IN MILLIMETERS SURFACE FINISH: TOLERANCES: LINEAR: ANGULAR:	FINISH:	DEBURR AND BREAK SHARP EDGES	DO NOT SCALE DRAWING	REVISION	
			FINAL YEAR PROJECT 2017		

	NAME	SIGNATURE	DATE
DRAWN			
CHK'D			
APPV'D			
MFG			
Q.A			

TITLE:

BLADE PROFILE NACA 65(4)221

MATERIAL:

DWG NO.

UNIT: Metre

A4

WEIGHT:

SCALE:1:8

SHEET 1 OF 1

Appendix D: Drawing for Blade Profile NACA 65(410)

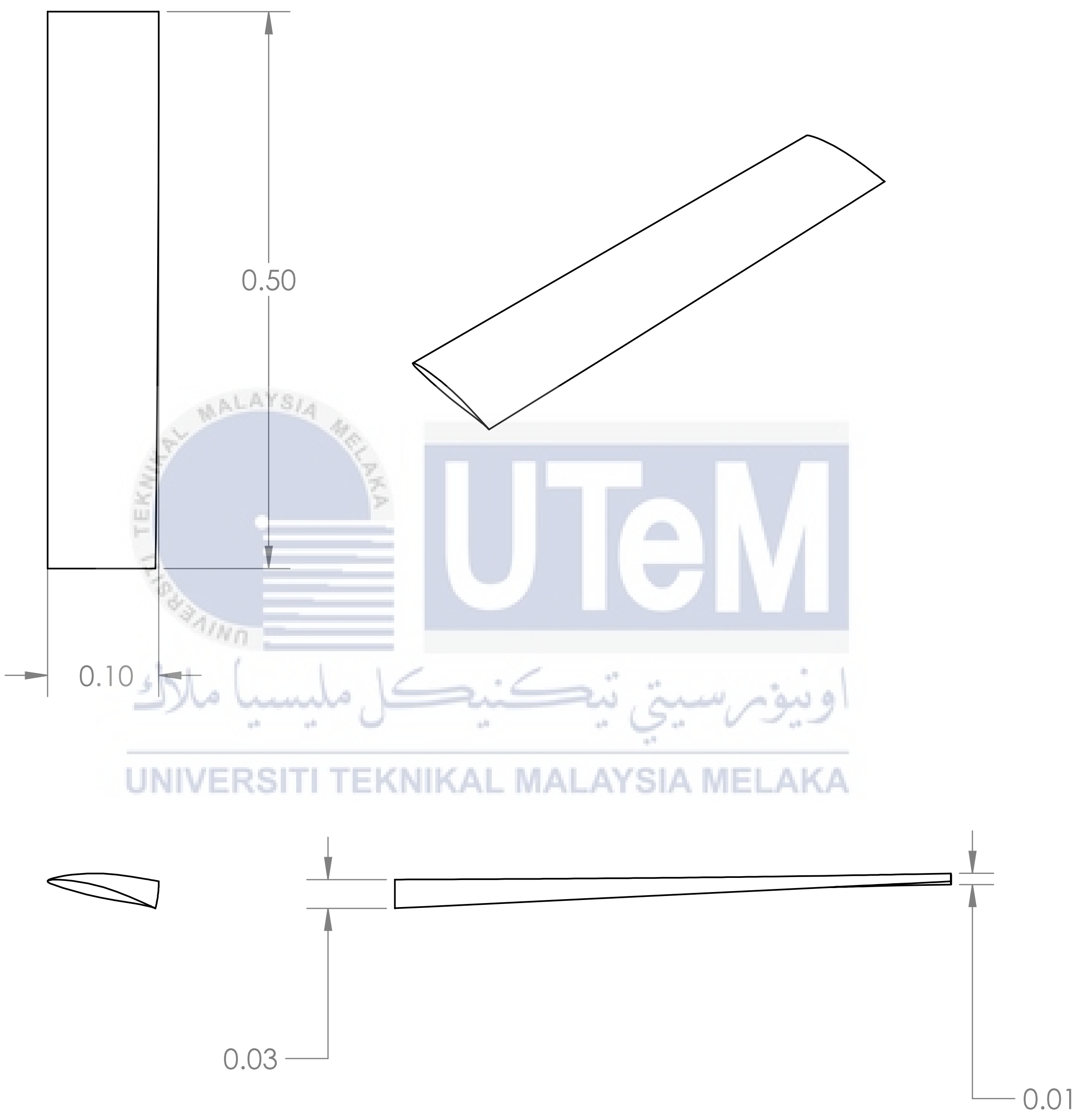

UNLESS OTHERWISE SPECIFIED:
DIMENSIONS ARE IN MILLIMETERS
SURFACE FINISH:
TOLERANCES:
LINEAR:
ANGULAR:

FINISH:

DEBURR AND BREAK SHARP EDGES

DO NOT SCALE DRAWING

REVISION

FINAL YEAR PROJECT 2017

	NAME	SIGNATURE	DATE
DRAWN			
CHK'D			
APPV'D			
MFG			
Q.A			

TITLE:

BLADE PROFILE
NACA 65(410)

MATERIAL:

UNIT: Metre

A4

WEIGHT:

SCALE:1:6

SHEET 1 OF 1